Chem Soc Rev

Fluorescent, MRI, and colorimetric chemical sensors for the first-row d-block metal ions

Journal:	*Chemical Society Reviews*
Manuscript ID:	CS-REV-08-2014-000285.R1
Article Type:	Review Article
Date Submitted by the Author:	30-Sep-2014
Complete List of Authors:	Peng, Xiaojun; State Key Laboratory of Fine Chemicals, Dalian University of Technology, Dalian University of Technology Zhu, Hao; Dalian University of Technology, State Key Laboratory of Fine Chemicals Fan, Jiangli; Dalian University of Technology, State Key Laboratory of Fine Chemicals Wang, Benhua; Dalian University of Technology, State Key Laboratory of Fine Chemicals

Cite this: DOI: 10.1039/c0xx00000x

www.rsc.org/xxxxxx

ARTICLE TYPE

Fluorescent, MRI, and colorimetric chemical sensors for the first-row d-block metal ions

Hao Zhu,[a] Jiangli Fan, *[a] Benhua Wang,[a] and Xiaojun Peng*[a]

Received (in XXX, XXX) Xth XXXXXXXXX 20XX, Accepted Xth XXXXXXXXX 20XX

DOI: 10.1039/b000000x

Transition metals (d-blocks) are recognized as playing critical roles in biology, and they most often act as cofactors in diverse enzymes; however, improper regulation of transition metal stores is also connected to serious disorders. Therefore, the monitoring and imaging of transition metals are significant for biological research as well as clinical diagnosis. In this article, efforts have been made to review the chemical sensors that have been developed for the detection of the first-row d-block metals (except Cu and Zn): Cr, Mn, Fe, Co, and Ni. We focus on the development of fluorescent sensors (fall into three classes: "turn-off", "turn-on", and ratiometric), colorimetric sensors, and responsive MRI contrast agents for these transition metals (242 references). Future work will be likely to fill in the blanks: 1) sensors for Sc, Ti, and V; 2) MRI sensors for Cr, Mn, Co, Ni; 3) ratiometric fluorescent sensors for Cr^{6+}, Mn^{2+}, and Ni^{2+}, explore new ways of sensing Fe^{3+} or Cr^{3+} without the proton interference, as well as extend applications of MRI sensors to living systems.

1. Introduction

Metals are indispensable for life, as they are involved in many fundamental biological processes, including osmotic regulation, catalysis, metabolism, biomineralization, and signalling[1]. The important metals in living organisms fall into two classes: the transition metals (e. g. Fe, Zn, Cu, Mn, Co, Ni, Mo, V, and Se) and the alkali and alkaline earth metals (e. g. Na, K, Ca, and Mg)[2]. The transition metals are present at much lower levels and often referred to as trace elements[1]. Because of their electronic structures (effective electrophiles), the transition metals most often act as cofactors in diverse enzymes[2], such as cytochrome oxidase, histidine ammonia-lyase, and glutamate mutase[3]. In the most cases, the metal in a metalloenzyme serves as a redox reagent. For example, catalase, a heme-iron-containing enzyme, catalyzes the breakdown of hydrogen peroxide, in which the Fe^{2+} acts as an electron exchanger and is reversibly oxidized and reduced[3]. On the other hand, misregulation of the quantity of these transition metals is connected to acute and long-term diseases, including heart disease, cancer and neurodegeneration[4]. Therefore, the assessment and understanding of metal distribution in living systems could be crucial to give more insight into metal homeostasis, as well as into its related diseases[4].

Chemical sensors are generally understood to be molecular devices that transform chemical information into analytically useful signals, such as electrical, electronic, magnetic, or optical signals[5]. A typical chemical sensor contains a receptor (the recognition site) linked to the signal source, such as a fluorophore, chromophore, or MRI contrast agent. Analyte recognition (binding or reacting) produces a change in the sensor properties (fluorescence, absorption, relaxivity *et al.*). For sensing metal ions, a small change in the receptor may cause a great difference in the selectivity[6] and sensing mechanism[7]. Fluorescent sensors have been developed to be a useful tool to sense *in vitro* and *in vivo* biologically important species including metal ions because of their specificity and sensitivity monitoring with fast response time[8]. Once the analyte is recognized by the receptor, the fluorescence signal can be observed in the form of quenching, enhancement or shift in the fluorescence maxima due to either electron transfer (eT), charge transfer (CT) or energy transfer (ET) processes[9-10]. Colorimetric sensors have also attracted much attention by which the detection of analytes can be carried out by the naked eye[11]. It allows on-site and real-time detection in an uncomplicated and inexpensive manner, offering qualitative and quantitative information[12]. In addition, MRI is a particularly powerful, clinically-used technique (since early 1980s) for molecular imaging[13]. The MRI contrast agents, Gd^{3+} complexes in the majority of cases, accelerate the relaxation of the surrounding water protons, which enhances the intrinsic contrast and thus the anatomical resolution of the MRI[14]. In recent years, there has been continuous interest in the development of responsive contrast agents that can report species of interest in living systems[4, 13, 15].

In this review, we focus on the development of fluorescent sensors, colorimetric sensors and responsive MRI contrast agents for the first-row d-block metals (except Cu and Zn): Cr, Mn, Fe, Co, and Ni. We note that Sc, Ti, and V not covered are also worthy of further investigation. The fluorescent sensors are categorized into three types: 1) "turn-off", 2) "turn-on", 3) ratiometric, which is, respectively, quenched, enhanced and shifted upon recognition of the target analyte. Given that

molecular and supramolecular fluorescent sensors for the detection of Fe^{3+} have been summarized by Sahoo *et al*[10] in 2012, our attention to the fluorescent Fe^{3+} sensors is given to contributions appearing in the 2012–2014 time period.

2. Chromium

Chromium, in the trivalent form (Cr^{3+}), is an important ingredient of a balanced human and animal diet[16], with a recommended daily intake 50–200 μg for adults[17]. The mechanism by which Cr^{3+} affects human metabolism is based on modulation of the action of insulin through glucose tolerance factors (GTF), thereby activating certain enzymes and stabilizing proteins and nucleic acids[18]. Chromium deficiency can increase the risk factors associated with diabetes, cardiovascular diseases, and nervous system disorders[19]. At elevated levels Cr^{3+} can bind to DNA negatively affecting the cellular structures and damaging the cellular components that may even lead to mutation and cancer[20]. Cr^{3+} can be oxidized to the more toxic species, hexavalent chromium (Cr^{6+}), which can penetrate cell membranes and may cause death to animals and humans if ingested in large doses by oxidizing DNA and some proteins[21].

2.1 Cr(III) sensors

Cr^{3+} is known to hydrolyze in water, forming its corresponding hydrates and hydroxides and releasing protons[22]. The pH of water can drop to around 4.53 when 500 μM Cr^{3+} is added[23]. While the hydrolysis of Cr^{3+} can be effectively inhibited in a buffer solution[23]. The majority of Cr^{3+} sensors, such as the ones based on photoinduced electron transfer (PET) or rhodamine are also sensitive to the proton. Therefore, it is better for Cr^{3+} sensors to work in a buffered aqueous solution, and testing the pH effect on the sensors' properties is necessary.

2.1.1 Fluorescent sensors for Cr(III)

"Turn-off" fluorescent sensors for Cr(III)

Tang and co-workers[24] developed a fluorescent reagent *o*-vanillin-8-aminoquinoline (**Cr-1**) for the determination of Cr^{3+}. In CH_3CN–H_2O (1:1, v/v) medium of pH 6.00, the formation of complex **Cr-1**-Cr^{3+} (1:1) caused static fluorescence quenching at $\lambda_{ex/em}$ = 280/314 nm due to the paramagnetic nature of Cr^{3+}. The difference of fluorescence intensity between **Cr-1** and complex was high and remained constant in the range over pH 5.2–8.3. Cr^{6+} could also be determined by reducing Cr^{6+} to Cr^{3+} with Na_2SO_3. In another approach, Das *et al*[25] reported a fluorescent ligand **Cr-2** for Cr^{3+} based on the affinity of hard binding sites (N, O) of acridone derivative towards Cr^{3+}. Upon addition of Cr^{3+} ion, quenching of the fluorescence intensity at 498.4 nm occurred in DMF–H_2O (9/1, v/v). The interference of foreign ions has been found to be negligible. Analysis of Cr species (Cr^{3+} and Cr^{6+}) in different synthetic as well as environmental samples has been performed.

"Turn-on" fluorescent sensors for Cr(III)

Photoinduced electron transfer (PET) is a long-range deactivation process in the form of an electron transfer from the ion-free receptor to the photoexcited fluorophore[26-27]. The PET-based mechanism is particularly attractive for the design of "turn-on" fluorescent sensors because of its simplicity[28]. In the ion-free situation, the fluorescence of the fluorophore is "switched off" by the PET process. However, arrival of the metal ion or the proton causes the fluorescence to be switched back "on" again due to the suppression of the PET process. A few "turn-on" fluorescent sensors have been reported for Cr^{3+} based on the PET mechanism.

Samanta *et al*[29] designed a Cr^{3+}-selective fluorescence sensor **Cr-3** in which the SNS (di(2-ethylsulfanylethyl)amine) ligand and 4-aminophthalimide were employed as a guest-binding unit and the fluorescing moiety, respectively. The fluorescence quantum yield of **Cr-3** in THF was measured to be 0.026 indicating PET between the fluorophore and receptor moieties. The coordination of **Cr-3** to Cr^{3+} caused an approximately 17-fold increase in the fluorescence quantum yield, which is attributed to the disruption of PET. However, an effective binding also occurred in the presence of Fe^{3+} with an approximately 4-fold increase. In another approach, a BODIPY-based fluorescent sensor (**Cr-4**) for Cr^{3+} bearing simple NO bidentate ligands was reported by Shiraishi *et al*[30]. **Cr-4** showed almost no fluorescence with a quantum yield (Φ_F) of 0.003 in CH_3CN. Addition of Cr^{3+} created a strong fluorescence (Φ_F = 0.69) at 643 nm and the 2:2 complex was the major emitting species.

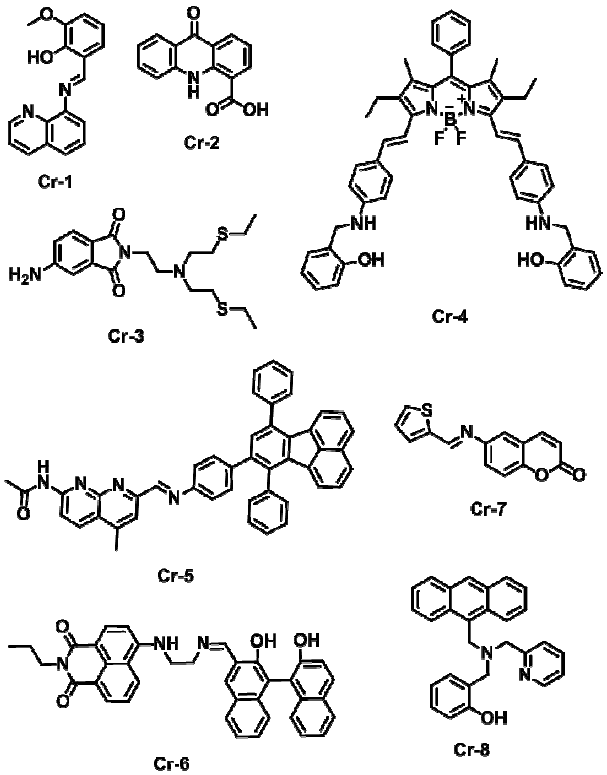

Zhang and co-workers[31] have developed a "turn-on" fluorescent sensor **Cr-5** for the selective signalling of Cr^{3+}, which consists of a naphthyridine moiety and a 7,10-diphenylfluoranthene moiety. Upon titration of Cr^{3+} in ethanol, a new fluorescent emission peak at about 447 nm appeared and the intensity dramatically enhanced, probably due to the prohibition of PET upon metal binding. Confocal laser scanning microscopy experiments have proven that **Cr-5** can be used to monitor intracellular Cr^{3+}. Sensor **Cr-6** reported by Wang *et al*[32] is based on naphthalimide and [1,1'-binaphthalene]-2,2'-diol (BINOL) framework. Free **Cr-6** exhibited a slight fluorescence response with a maximum at 491 nm (Φ = 0.08) in THF–H_2O (85:15, v/v).

Upon addition of Cr^{3+}, fluorescence enhancement and a slight red-shift of emission band centered at 498 nm were observed (Φ = 0.27). Das *et al*[33] have introduced a thiophene-coumarin hybrid molecule (**Cr-7**), which behaved as a Cr^{3+}-selective fluorescent sensor in CH_3CN–HEPES buffer (4:6, v/v, pH 7.4). Addition of Cr^{3+} to the solution of **Cr-7** resulted in the enhancement of fluorescence intensity at 550 nm. Cr^{3+} assisted restricted rotation around the imine bond and inhibited PET from the N, S-donor sites to the coumarin unit were responsible for the fluorescence enhancement. **Cr-7** was employed to monitor Cr^{3+} in *Candida albicans cells*. By the combination of an anthracene group as a chromophore moiety and a phenol group as a binding moiety, Kim group[34] developed a "turn-on" fluorescent sensor **Cr-8** for trivalent cations (Al^{3+}, Cr^{3+}, Fe^{3+}, Ga^{3+}, and In^{3+}) with a prominent fluorescence enhancement and a slight red shift of the emission maxima from 411 to 421 nm.

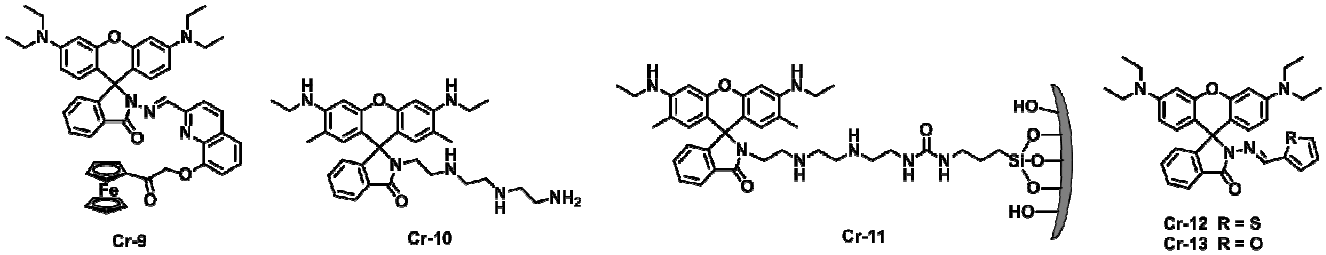

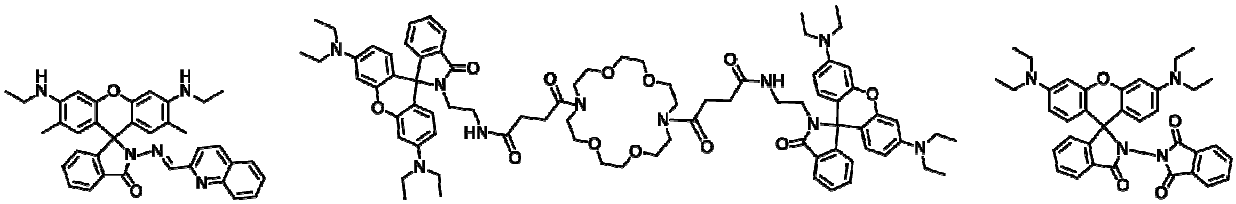

Rhodamine dyes have been extensively used as fluorophores by virtue of their excellent photophysical properties, such as long absorption and emission wavelengths, high fluorescence quantum yield, large absorption coefficient, and exceptional stability against photobleaching. Furthermore, rhodamine frameworks have been considered as an ideal mode for the construction of the "turn-on" systems based on the structural change of the rhodamine moiety from spirocyclic to ring-opened forms[35-36]. The spirocyclic form is basically colorless and non-fluorescent, whereas ring-opening of the corresponding spirolactam by the addition of H^+ or metal ions gives rise to strong fluorescence emission and a pink color. Next we will summary the Cr^{3+}-selective rhodamine-based sensors.

Li *et al*[37] have introduced a multisignal sensor (**Cr-9**) for Cr^{3+} based on rhodamine B with a ferrocene substituent. Upon binding with Cr^{3+}, the absorption peak of **Cr-9** at 565 nm and the emission peak at 587 nm increased in intensity evidently in C_2H_5OH–H_2O (1:1, v/v, pH 7.4), clearly indicating the ring-opening process of the rhodamine B unit in **Cr-9**. The detection of Cr^{3+} by **Cr-9** could work in the pH range of 5.0–10.0. In addition, **Cr-9** showed a distinct current change of the electric currency in its reversible ferrocene/ferricinium redox cycles upon complexation with Cr^{3+}. In the selectivity test, Hg^{2+} elicited a slight fluorescence enhancement except Cr^{3+}, while the other metal ions did not cause any discernible changes. By means of confocal laser scanning microscopy experiments, **Cr-9** was used as a fluorescent sensor for monitoring Cr^{3+} in HeLa cells.

Sensor **Cr-10** was facilely synthesized from the reaction of rhodamine 6G with triethylenetetramine by Mao *et al*[6, 38]. **Cr-10** formed nearly colorless and non-fluorescent in HEPES aqueous buffer solution (pH =7.2). With the addition of Cr^{3+}, the typical absorbance (527 nm) and fluorescence (552 nm) of rhodamine 6G appeared, resulting from the ring-opened form of **Cr-10**. The fluorescence intensity enhancement of this system was linearly proportional to Cr^{3+} concentration from 5.0×10^{-8} to 7.0×10^{-6} M with a detection limit of 1.6×10^{-8} M. Besides, the spirocyclic form of **Cr-10** was stable between pH 5.5–8.5 with a minute fluorescence intensity. By immobilizing **Cr-10** within the channels of SBA-15, Duan *et al*[39] prepared a dye-functionalized silica nanomaterial, sensor **Cr-11**, for the determination of Cr^{3+} in water. Upon addition of Cr^{3+}, **Cr-11** showed strong fluorescence with an approximately 8-fold enhancement in the intensity at 553 nm. The Cr^{3+}-loaded **Cr-11** after isolation from the aqueous suspension underwent a color change from almost colorless to pink. Through isolating of the metal ions within the mesopores of the silica, **Cr-11** can extract Cr^{3+} from the solution with only trace amounts remaining. **Cr-11** was cell-permeable and could be used to monitor Cr^{3+} in HeLa cells. Moreover, the functional material was successfully taken up into various parts, especially the head, of the zebrafish and a strong red fluorescence was emerged in the presence of external Cr^{3+} ions.

Sinn *et al*[40] presented sensor **Cr-12** which was capable of sensing Cr^{3+} *via* the carbonyl O, inamine N, and thiophene S as the binding sites. In CH_3CN, addition of Cr^{3+} resulted in a remarkably enhanced fluorescence at 583 nm accompanied by color changes from colorless to pink. However, sensor **Cr-12** also showed some fluorescence responses toward Hg^{2+}, Zn^{2+} and Pb^{2+}. By displacing thiophene with furfuran, another rhodamine-based Cr^{3+} sensor (**Cr-13**) was developed by Niu *et al*[41]. The spectroscopic investigations were carried in Tris-HCl (10 mM) aqueous buffer solution. **Cr-13** also displayed obvious fluorescence and absorption changes in the presence of Cr^{3+} with a working pH range of 5.0–9.0. Analysis of confocal images of Cr^{3+} utilizing **Cr-13** indicates that the sensor was cell permeable

and capable of sensing Cr^{3+} in Arabidopsis guard cells and PC12 cells.

Sensor **Cr-14**, containing a quinoline ligand and developed by Das *et al*[42] showed remarkable preference toward Hg^{2+} and Cr^{3+}. The spirocyclic form for **Cr-14** was retained for a pH range of 5.0–11.0 in a CH_3CN–HEPES buffer (3:2, v/v, pH 7.3) medium. **Cr-14** allowed detection of Hg^{2+} and Cr^{3+} by monitoring changes in the absorption and fluorescence spectral pattern. Further, **Cr-14** was used as an imaging reagent for detection of Hg^{2+} and Cr^{3+} uptake in MCF-7 cells using laser confocal microscopic studies. By linking two rhodamine B moieties to the two amine sides of a 4,13-diaza-18-crown-6 ether, Bao and co-workers[43] developed a fluorescent sensor **Cr-15** for monitoring Cr^{3+}. In a CH_3OH–H_2O (3:2, v/v, pH 7.2) solution, sensor **Cr-15** formed a 1:2 complex with Cr^{3+} resulting in absorption and fluorescence enhancement at 560 nm and 582 nm, respectively. In addition, **Cr-15** was cell-permeable and used to detect Cr^{3+} in human L-02 hepatocytes. Sensor **Cr-16** developed by Das *et al*[44] was found to bind specifically to Hg^{2+} and Cr^{3+} with a "turn-on" response at 531 nm for absorption spectra and at 557 nm for fluorescence spectra in CH_3CN–HEPES buffer (1:1, v/v, pH 7.2).

In addition, some other attempts have been reported for the selective determination of Cr^{3+} by means of chelation-enhanced fluorescence (CHEF). By combining a dansyl unit as the fluorophore and carboxhydrazone derivatives as the ionophores into one conjugated molecule, Duan *et al*[45] developed two fluorescent sensors (**Cr-17** and **Cr-18**) for Cr^{3+}. **Cr-17** contained a pyridine-carboxhydrazone tridentate coordination site, forming a 2:1 stoichiometric complexation species with Cr^{3+}, and exhibited selectivity for Cr^{3+} over other metal ions in DMF–H_2O (9:1, v/v) solution. **Cr-17** displayed high quantum yield (Φ = 0.86) and fluorescence enhancement following Cr^{3+} coordination within a pH range of 5.0 to 9.0. **Cr-18** contained a 8-hydroxyquinoline-carboxhydrazone tetradentate metal-binding moiety, forming a 1:1 complex with Cr^{3+}. **Cr-18** also exhibited fluorescence enhancement but a much lower quantum yield (Φ = 0.059) after Cr^{3+} binding.

Yoon *et al*[46] reported two thiazolothiazole derivatives (**Cr-19** and **Cr-20**) as fluorescent sensors for Cr^{3+} and Al^{3+}, in which ether binding units were introduced. The photophysical properties of **Cr-19** and **Cr-20** were tested in CH_3CN–$CHCl_3$ (4:1, v/v) and CH_3CN, respectively. **Cr-19** showed large fluorescence enhancement with Cr^{3+} and Al^{3+} while Fe^{2+}, Cu^{2+} and Pb^{2+} induced relatively smaller enhancement. **Cr-20** bearing longer ethylene oxide unit showed selective fluorescence "turn-on" change upon the addition of Cr^{3+}, though Al^{3+} gave a mild response. Gil *et al*[47] introduced a phenanthrene-based bis-oxime sensor **Cr-20** for Fe^{3+} and Cr^{3+} discrimination in which oxime groups act as ligands for cation complexation. Addition of Cr^{3+} gave rise up to a 62% fluorescence enhancement of **Cr-20** in DMSO–CH_3OH (9:1, v/v) solution in the 1:2 complex. However, fluorescence quenching was observed in the presence of Fe^{3+} with the 1:1 complex.

Goswami *et al*[48] have developed a spirobenzopyran derivative (**Cr-22**) applied in simultaneous colorimetric and NIR fluorescence detection of Cr^{3+}. This spirobenzopyran receptor was normally colorless and weak fluorescent (Φ = 0.006) in CH_3CN–HEPES buffer (7:3, v/v, pH 7.4), but the formation of merocyanine occurred by Cr^{3+} showing a yellow color (λ_{abs} = 440 nm) and strong NIR fluorescence emission (Φ = 0.161) at 675 nm. The observed dramatic fluorescence enhancement could be a result of the combination effect of intramolecular charge transfer (ICT) and CHEF. The only cross interfering metal ion Cu^{2+} caused a new peak at 555 nm in the UV-vis spectra and it behaved as a fluorescence quencher in emission spectra. The fluorescence sensitivities of **Cr-22** towards Cr^{3+} become maximum at pH 7.4. **Cr-22** could permeate the plasma membrane and give specific fluorescence with Cr^{3+} in HeLa cells.

Chattopadhyay and co-workers[49] designed a fluorescent Cr^{3+} receptor, **Cr-23**, which underwent a solvent assisted 1,5-σ tropic shift leading to a benzimidazole derivative (**Cr-23'**) of more chelating environment in the presence of Cr^{3+} and exhibited moderate fluorescence intensity due to internal electron transfer process. This sensor behaved a "turn-on" response at 426 nm for Cr^{3+} in C_2H_5OH–HEPES buffer (1:5, v/v, pH 7.4), presumably due to the CHEF effect during chelation of **Cr-23'** toward the Cr^{3+} in a 1:1 complex mode. Other metal ions did not interfere except Cu^{2+}. Sensor **Cr-23** was used to image Cr^{3+} in HeLa cells with low cytotoxicity.

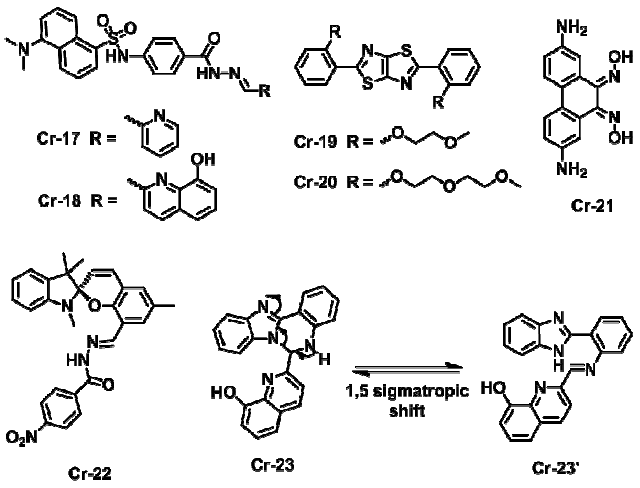

Ratiometric fluorescent sensors for Cr(III)

Measuring fluorescence by a decrease or increase in the emission intensity without much shift of either excitation or emission wavelength can be influenced by many factors, such as the sensor concentration, changes of environment around the sensor (pH, polarity, temperature, and so forth), and the instrumental efficiency[50]. To reduce these effects, ratiometric measurement is utilized, namely, simulaneous recording of the fluorescence intensities at two wavelengths and calculation of their ratio[51]. Several signalling mechanisms, such as ICT, excimer/exciplex formation, excited state intramolecular proton transfer (ESIPT), fluorescence resonance energy transfer (FRET), and through-bond energy transfer (TBET).

On the basis of FRET from 1,8-naphthalimide to rhodamine, Li *et al*[52] developed a fluorophore dyad (**Cr-24**) as a Cr^{3+}-selective fluorescent sensor. Upon addition of Cr^{3+} to **Cr-24** in C_2H_5OH–H_2O (2:1, v/v) solution, the fluorescence intensity at 544 nm (λ_{ex} = 405 nm) gradually decreased and that of a new fluorescent band centered at 592 nm gradually increased. This is consistent with increased FRET from 1, 8-naphthalimide (donor)

to the ring-open form of rhodamine (acceptor). Alkali and alkaline-earth metal ions gave no interference, whereas Ag^{+}, Ni^{2+}, Cd^{2+}, Hg^{2+}, Fe^{2+}, Pb^{2+}, and Al^{3+} gave a weak response. **Cr-24** was applied to detect intracellular Cr^{3+} with the FRET method under excitation at 405 nm. Moreover, the two-photon spectral response of **Cr-24** to its interaction with Cr^{3+} ions was investigated by Xia *et al*[53]. A 29-fold enhancement of two-photon excited (λ_{ex} = 850 nm) fluorescent intensity at 583 nm was observed when 10 eq. Cr^{3+} was added to the **Cr-24** solution. The two-photon excited fluorescence "turn-on" behavior further extended the excitation to near infrared regime, and showed more effective sensitivity.

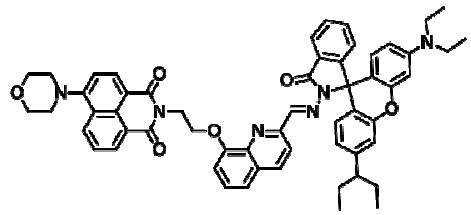

Cr-24

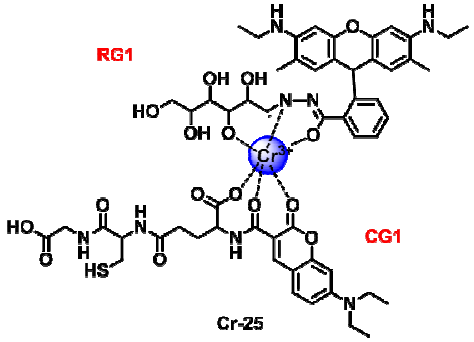

Cr-25

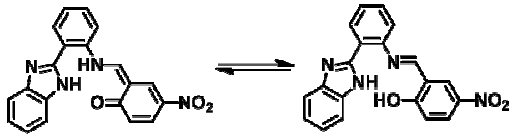

Cr-26

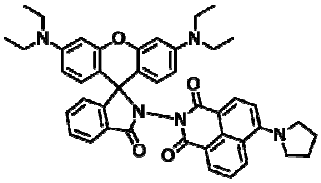

Cr-27

Duan *et al*[54] designed a simple FRET-based approach to ratiometric fluorescence sensing of Cr^{3+} in aqueous solution using glutathione and glucose as building blocks, inspired by the binding motifs of Cr^{3+} in GTF. Glutathione-based receptor (**CG1**) and glucose-based receptor (**RG1**) were combined into one system **Cr-25** for sensing Cr^{3+}. Upon gradual addition of Cr^{3+} ions in NaAc-HAc buffer solution (pH = 6.0), the intensity of the emission band centered at 475 nm decreased and that of a new fluorescent band centered at 555 nm increased. No significant spectral changes were observed in the presence of the other metal ions except Hg^{2+} which induced a 2-fold fluorescence enhancement. Confocal experiments revealed that the combined **CG1** and **RG1** with Cr^{3+} ions exhibited green fluorescence signals localized in the perinuclear region of the cytosol in MCF-7 cells. Unfortunately, the ratiometric sensing of Cr^{3+} in living cells by this system was not obtained.

An imine-linked, benzimidazole-based sensor **Cr-26**, reported by Jang *et al*[55], was used for chromogenic recognition of Mg^{2+} and fluorescent recognition of Cr^{3+}. Addition of Mg^{2+} to a solution of **Cr-26** in CH_3CN–HEPES buffered (8:2, v/v, pH 7.0) led to a stepwise decrease in absorbance at 400 nm and an increase at 350 nm with a clear isosbestic point at 385 nm. Cr^{3+} binding with sensor **Cr-26** caused a change in the fluorescence spectra of **Cr-26** with quenching at 415 nm and enhancement at 475 nm. In the absence of Cr^{3+}, the enol form of **Cr-26** was in equilibrium with its keto tautomer in the excited state. The modulation of the fluorescence spectrum of **Cr-26** with the addition of Cr^{3+} was due to the formation of a stable Cr^{3+} complex with the keto form of **Cr-26**. In addition, **Cr-26** was applicable for staining the cytoplasm of microbial cells enriched with Cr^{3+}. Das *et al*[44] have presented a rhodamine derivative **Cr-27** used as a ratiometric sensor for the detection of Cr^{3+} and Hg^{2+} based on the FRET process involving the donor naphthalimide (λ_{abs} = 455 nm, λ_{em} = 533 nm) and the receptor Cr^{3+}/Hg^{2+}-bound xanthenes fragment (λ_{abs} = 561 nm, λ_{em} = 583 nm). Moreover, when used on epithelial cells like A431, the reagent **Cr-27** could detect the cellular uptake of Cr^{3+} or Hg^{2+}.

2.1.2 Colorimetric sensors for Cr(III)

By the coupling of 8-aminoquinoline and 1-hydroxynaphthalene-2-carbaldehyde, Kim group[56] developed a selective colorimetric sensor **Cr-28** for Cr^{3+}. Upon the addition of Cr^{3+} into the CH_3OH solution of **Cr-28**, the absorption bands at 278, 344, 467, and 494 nm significantly decreased, and two new bands at 262 and 382 nm appeared. Meanwhile, the solution color changed from yellow to colorless. In the presence of other metal ions, **Cr-28** showed either no change or a slight decrease in the absorption intensity except Fe^{2+} which induced a slight blue shift.

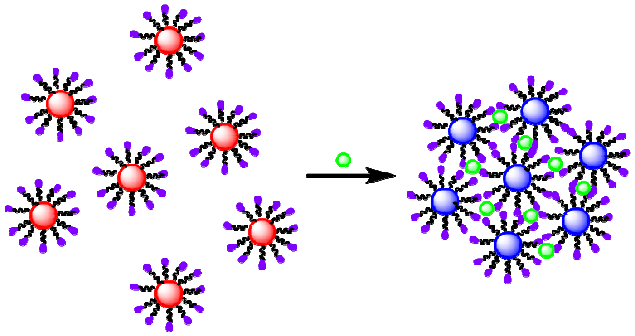

Scheme 1 Schematic depiction of AuNP-based colorimetric assays for metal ions.

Plasmonic nanoparticles, such as gold nanoparticles (AuNPs) and silver nanoparticles (AgNPs), are a class of nanostructures whose optical properties are determined by their unique surface plasmon resonance (SPR)[57]. The SPR of gold, for instance, exhibits a colorimetric behavior (red to blue) directly tuned by altering the interparticle distance and the size, shape, and

composition of particles, which is suited for naked-eye assays[58] (Scheme 1). AuNPs possess distinct physical and chemical attributes: 1) ease of synthesis and monodispersity in aqueous media with large surface-to-volume ratio; 2) biocompatibility and ease of chemical functionalization through surface chemistry; 3) high absorption extinction coefficient (*ca.* 10^8 $cm^{-1}M^{-1}$) and strong photostability[59]. So far, several excellent AuNP-based colorimetric assays have been developed and widely applied in chemical and biological detection[60-63].

Zhu and co-workers[64] have developed a colorimetric technique for the determination of Cr^{3+} in aqueous solution based on an aggregation-induced color transition of AuNPs. AuNPs were functionalized with a dithiocarbamate-modified *N*-benzyl-4-(pyridine-4-ylmethyl)aniline ligand (**Cr-29**) for the chelation of Cr^{3+}. A solution of the modified AuNPs displayed a SPR absorption peak at 520 nm and showed a wine-red color. When Cr^{3+} was added, the absorbance at 520 nm decreased with the appearance of a new absorption band at around 630 nm, and the color changed to blue, indicating rapid aggregation of the AuNPs. In another approach, Wu *et al*[65] synthesized triazole functionalized AuNPs (**Cr-30**) through a click reaction for selective colorimetric Cr^{3+} detection. Aggregation of **Cr-30** was induced immediately in the presence of Cr^{3+} ions, yielding an absorption peak shift from 526 nm to 639 nm which could be observed by the naked eye as a color change from red to blue. The optimal pH range for detecting Cr^{3+} by **Cr-30** is 4.0–7.0.

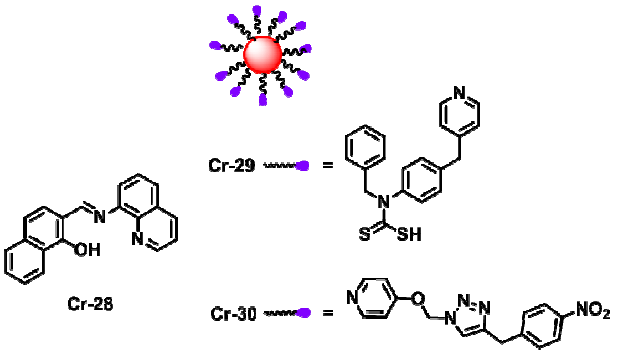

2.2 Cr(VI) sensors

2.2.1 Fluorescent sensors for Cr(VI)

"Turn-off" fluorescent sensors for Cr(VI)

Jie and co-workers[66] developed a fluorescence quenching method to determine chromium based on the oxidation of rhodamine 6G by $Cr_2O_7^{2-}$. The linear calibration graph was obtained in the range 8–80 ng mL^{-1} $Cr_2O_7^{2-}$ and the detection limit was 0.8 ng mL^{-1}. Most of foreign ions do not interfere in the determination of $Cr_2O_7^{2-}$ except Ce^{4+} and nitrite ions. The optimum fluorescence quenching occurred in the presence of H_2SO_4 in the range 0.25–0.75 mol/L. Arnold *et al*[67] described a flow injection method for the measurement of $Cr_2O_7^{2-}$ in aqueous solutions based on the dynamic fluorescence quenching of a ruthenium (II) complex (**Cr-31**). The detection limit was 0.43 ppm. Some interference quenching was measured for cyanide and nitrate. The optimal working pH is at 8.0.

Compared to small organic molecules, the organic nanoparticles simultaneously provide efficient fluorescence, a great reduction in photobleaching, colloidal stability in a variety of environments. Based on the fluorescence quenching of organic nanoparticles of 4-vinlyanline[68] (**Cr-32**) or 1-pyrenemethylamine[69] (**Cr-33**) by $Cr_2O_7^{2-}$, two methods for the determination of $Cr_2O_7^{2-}$ were developed by Wang and co-workers[68-69]. The fluorescence intensities of these nanoparticle sensors were quenched in the presence of $Cr_2O_7^{2-}$, while H_2SO_4 was required for the sensing. They both showed high selectivity

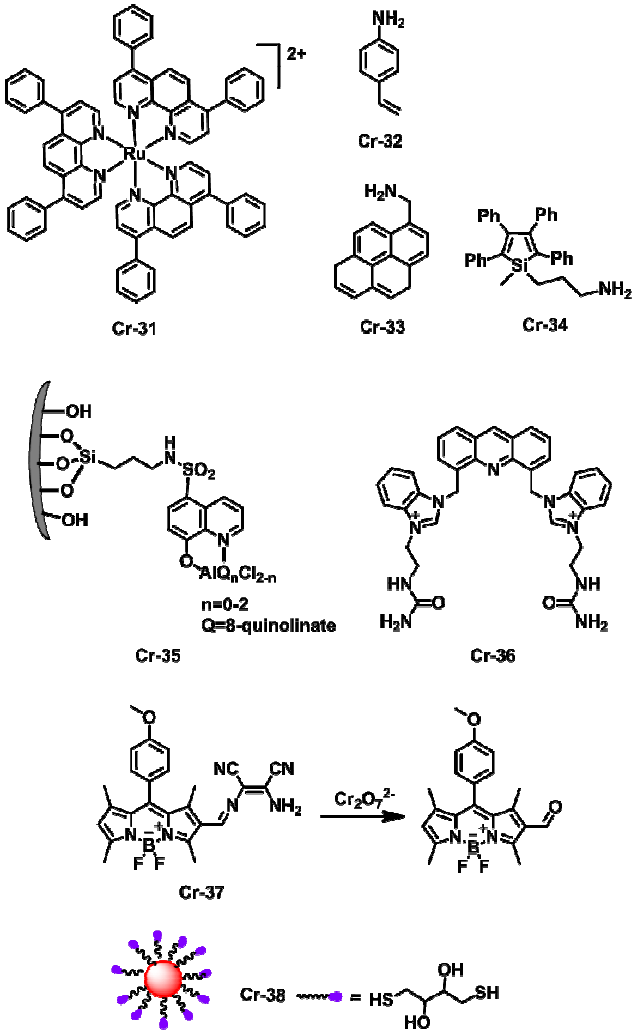

toward $Cr_2O_7^{2-}$ except that H_2O_2, HNO_2, $KMnO_4$, $KBrO_3$ and NaClO influenced the determination by **Cr-33**-based nanopariticle sensor. In another approach, Trogler and co-workers[70] reported a fluorescent silole sensor **Cr-34** for CrO_4^{2-} and AsO_4^{3-} by functionalization of a silole monomer with anion binding groups. Upon addition of CrO_4^{2-} and AsO_4^{3-} to the nanoparticle suspensions of **Cr-34**, the decrease in the fluorescence intensity at 485 nm was observed, which was due to electron transfer from the excited state of the silole to the analyte. Since AsO_4^{3-} is a weaker oxidant than CrO_4^{2-}, it is a weaker quencher as well. The colloid sensor in a pH 7 phosphate-buffered suspension shows both higher sensitivity and greater selectivity to CrO_4^{2-} than other oxoanion interferents, such as NO_3^-, NO_2^-, SO_4^{2-}, and ClO_4^-. By assembly of fluorescent aluminium complex of 8-hydroxyquionline (AlQ_x) within the channels of modified SBA-15, Hosseini *et al*[71] have developed a fluorescence nanosensor **Cr-35** for $Cr_2O_7^{2-}$ with working pH at 4.0. When the titrations with $Cr_2O_7^{2-}$ were performed, a

significant decrease in the fluorescence intensity at 486 nm was obtained. The lowest limit of detection was found to be 0.2 ng/mL.

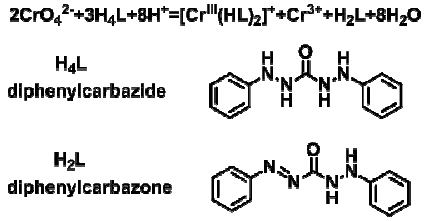

Scheme 2 Reaction of CrO_4^{2-} with diphenylcarbazide to generate a chelate of Cr^{3+} and diphenylcarbazone.

Inner filter effect (IFE) of fluorescence results from the absorption of the excitation and/or emission light by absorbers. Actually it is a source of error in fluorimetry, but a few IFE-based sensors have been developed. Ren *et al*[72] reported a fluorimetric method for determination of CrO_4^{2-} based on IFE of upconversion luminescent nanoparicles ($NaYF_4$: Yb^{3+}, Er^{3+}) as luminescent sensors. The principle of this assay is based on the complementary overlap of the green emission band of nanoparticles ($NaYF_4$: Yb^{3+}, Er^{3+}) with the absorption spectrum of a pink chelate complex (Cr^{3+}-diphenylcarbazone), which was generated by the quantitative reaction between diphenylcarbazide and CrO_4^{2-} in mineral acid solution (Scheme 2). The decrease in the upconversion luminescent nanoparticles was proportional to the concentration of CrO_4^{2-} in the range of 0.07–10.0 × 10^{-6} M and the detection limit is 2.40 × 10^{-8} M. Gao *et al*[73] developed another IFE-based sensor **Cr-36** for the detection of $Cr_2O_7^{2-}$. Upon addition of $Cr_2O_7^{2-}$ to aqueous solution at pH 6.1 of sensor **Cr-36**, the emission intensity at 437 nm decreased significantly when excited at 259 nm, which was ascribed to the strong absorption of $Cr_2O_7^{2-}$ to both the excitation and emission light of the acridine fluorophore. The fluorescence changes induced by other anions were negligible except for MnO_4^- which also has IFE on **Cr-36**. It is noteworthy that the sensing property of **Cr-36** toward $Cr_2O_7^{2-}$ was pH-insensitive (measurements with similar results were carried out at pH 4.0, 6.1 and 10.0).

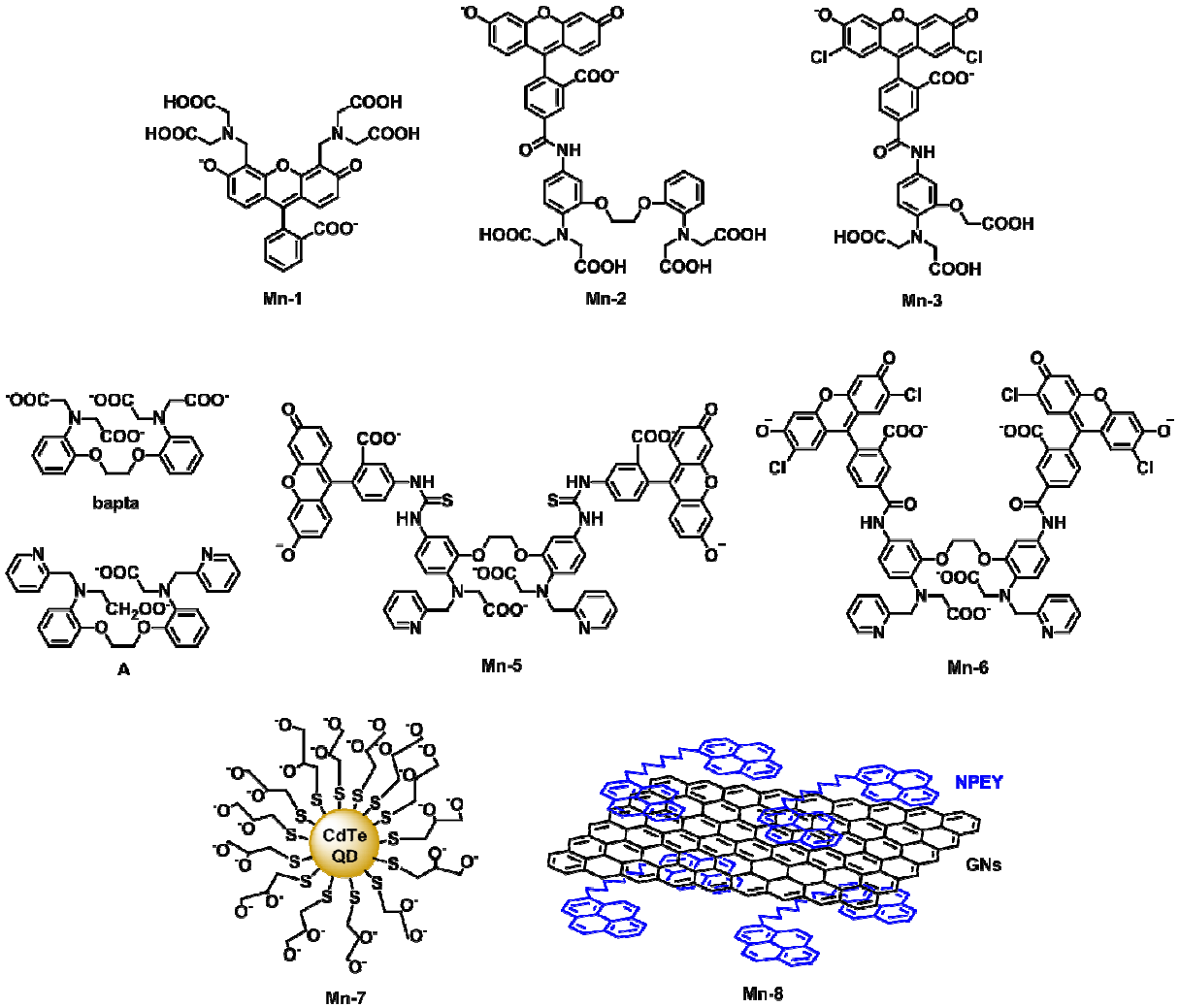

"Turn-on" fluorescent sensors for Cr(VI)

Tong and co-workers[74] have developed a fluorogenic method for the determination of $Cr_2O_7^{2-}$ based on the oxidation of non-fluorescent rhodamine B hydrazide by $Cr_2O_7^{2-}$ in acidic aqueous conditions to give highly fluorescent rhodamine B. The fluorescence enhancement at 585 nm was linearly related to the concentration of $Cr_2O_7^{2-}$ in the range of 5.0 × 10^{-8} to 2.0 × 10^{-6} M with a detection limit of 5.5 × 10^{-9} M. However, this method is

invalid in the absence of H_2SO_4. In another approach, Ye *et al*[75] reported a BODIPY based "turn-on" fluorescent chemodosimeter **Cr-37** integrated with diaminomaleonitrile unit for the detection of $Cr_2O_7^{2-}$. Sensor **Cr-37** displayed a rather weak fluorescence at 507 nm in DMF–PBS buffer (7:3, v/v, pH 6.8). Addition of $Cr_2O_7^{2-}$ induced strong fluorescence, which can be ascribed to the de-diaminomaleonitrile leading to aldehyde by $Cr_2O_7^{2-}$. **Cr-37** is cell membrane permeable and capable of fluorescent imaging of $Cr_2O_7^{2-}$ in living cells.

2.2.2 Colorimetric sensors for Cr(VI)

Tan *et al*[76] reported a colorimetric detection method based on 1,4-dithiothreitol functionalized AuNPs (**Cr-38**) for $Cr_2O_7^{2-}$ in aqueous solution. Addition of $Cr_2O_7^{2-}$ to the solution of **Cr-38** at pH 2.5 caused a notable red-shift (from 520 nm to 650 nm) of the SPR peak and a rapid color change from rose-red to blue-purple, which reflected the aggregation of **Cr-38** in the presence of $Cr_2O_7^{2-}$. Under the optimized conditions, a good linear relationship was obtained between the ratio ($A_{650/520}$) and the concentration of $Cr_2O_7^{2-}$ over the range of 100–600 nM, and the detection limit was 20 nM. This method showed selective detection towards $Cr_2O_7^{2-}$ against other common metal ions in water.

3. Manganese

Manganese is an essential transition metal that is required by organisms ranging from simple bacteria to humans[77]. Manganese plays a critical role in multiple bodily functions including immunity, regulation of blood sugars and cellular energy, blood clotting, reproduction, digestion, and bone growth. The best-known manganese-containing polypeptides may be arginase, the diphtheria toxin, and Mn-containing superoxide dismutase (Mn-SOD)[78]. The majority of manganese is thought to be present as low molecular-weight Mn^{2+} complexes[79]. The normal concentration of Mn^{2+} in organisms is very low, for instance 6–19 μg/L in the human blood[80]. However, chronic overexposure of Mn^{2+} can result in movement disorders and mental disturbances and other brain-related toxicities[81].

3.1 Fluorescent sensors for Mn(II)

Several commercially available chelating dyes produce strong fluorescence changes upon binding Mn^{2+}, e.g. **Mn-1** (**Calcein**) gave significant quenching towards Mn^{2+}, while **Mn-2** (**Calcium Green**) and **Mn-3** (**Magnesium Green**) exhibited markedly fluorescence enhancement in the presence of Mn^{2+}[82]. However, these dyes are also sensitive to other metal ions such as Ca^{2+} and Mg^{2+}. Recently, one method of ratiometric fluorescence detection (**Mn-4**) of Mn^{2+} was described by Canary and co-workers[83] based on a supramolecular metal displacement assay. Two commercially available dyes, calcein blue (**CB**) and fluozin-1 (**Fz1**), and Cd^{2+} were employed in the sensing system. Initially, Cd^{2+} was chelated by the strong ligand **CB** and the formed complex was strongly fluorescent, while free ligand **Fz1** gave weak fluorescence. Added Mn^{2+} competed with Cd^{2+} for **CB**, and quenched **CB**. Simultaneously, Cd^{2+} formed a complex with ligand **Fz1** whose fluorescence was consequently "turned on". The method was applied to detect Mn^{2+} in HEK and *DMT-1* cells treated with exogenous Mn^{2+}. Unfortunately, Cu^{2+} and Zn^{2+} showed obvious interference in the detection of Mn^{2+}.

In addition, Canary and co-workers[84] rationally designed a ligand **A** from bapta, a known Ca^{2+}-selective ligand that serves as the chelating moiety of calcium green[85], using a "soft atom poisoning" strategy to differentiate binding affinities to Mn^{2+} and Ca^{2+}. Binding preferences were tuned by substitution of carboxylate groups of bapta with pyridines, resulting in much stronger Mn^{2+} selectivity over Ga^{2+}. Ligand **A** was further functionalized to include a fluorescein fluorophore to realize the goal of fluorescent Mn^{2+} sensors (**Mn-5** and **Mn-6**). When excited at 493 nm, **Mn-5** showed an emission maximum at 519 nm. Upon addition of Mn^{2+}, an enhanced fluorescence was observed until saturation after 1 equivalent. Screening for selectivity against other metal ions showed no effect on fluorescence intensity of **Mn-5**, except Ca^{2+} which caused fluorescence enhancement at higher concentration. Sensor **Mn-6** showed a longer λ_{em} (530 nm) due to the two incorporated chlorine atoms on the fluorophore, and maintained high selectivity towards Mn^{2+}. Furthermore, the ester precursor of sensor **Mn-6** was used for Mn^{2+} detection in live cells.

Cui and co-workers[80] reported a pH-controlled recognition method for the discriminative detection of Mn^{2+} and Cu^{2+} ions *via* 1-thioglycerol (TG)-capped CdTe QD (**Mn-7**) fluorescence sensing. The sensitivity of **Mn-7** to Mn^{2+} strongly depends on the solution pH. No obvious fluorescence alteration occurred after the addition of Mn^{2+} into a pH 8.2 buffer solution, whereas a dramatic fluorescence decrease appeared at pH 11.0 with a detection limit of 10 nM. In comparison, the detection of Cu^{2+} was subject to a minor impact of solution pH. Therefore, the recognizable detection of Mn^{2+} and Cu^{2+} could be realized by adjusting the solution pH. The peculiar pH-controlled sensitivity to Mn^{2+} was attributed to the pH-dependent diffusion and absorption of Mn^{2+} on the surface of **Mn-7** and the energy transfer from CdTe QDs to Mn^{2+}.

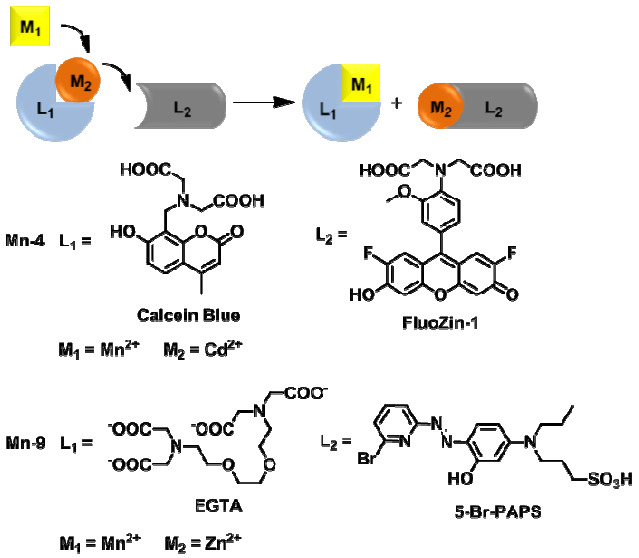

Li and co-workers[86] have developed a simple and convenient route for processing "turn-on" fluorescence sensor **Mn-8** for Mn^{2+} recognition: pyrene derivative ethane (NPEY) utilized as ideal fluorescent reporting groups for heavy metal ions, was brought to the surface of graphene nanosheets (GNs) *via* π-π stacking. The spectrum of the free **Mn-8** showed two weak

emission bands at 376 and 396 nm, which could be the result of fluorescence quenching through the PET process. Among various heavy metal ions, only Mn^{2+} induced a dramatic increase in the fluorescence intensity of **Mn-8**. This sensor could be used to image intracellular Mn^{2+} in live cells by using confocal fluorescence microscopy.

3.2 Colorimetric sensors for Mn(II)

Some early colorimetric methods[87-90] have been used to detect Mn^{2+} based on photochemical oxidation reactions catalyzed by Mn^{2+}. Recently, Dai *et al*[91] have developed a visible color displacement system (**Mn-9**) for the colorimetric and ratiometric detection of Mn^{2+} ions, which is composed of 2-(5-bromo-2-pyridylazo)-5-[*N*-propyl-*N*-(3-sulfopropyl)amino]phenol (5-Br-PAPS), ethylene glycol-bis(2-aminoethylether)-*N*, *N*, *N'*, *N'*-tetraacetic acid (EGTA) and Zn^{2+} at neutral pH. Upon presentation of Mn^{2+}, Zn^{2+} is displaced from EGTA to bind 5-Br-PAPS to produce a pronounced color change from yellow to purple. The absorbance decreases at 449 nm and increases at 552 nm, both linearly to Mn^{2+} concentration at low micromolar levels.

4. Iron

Iron is the most abundant transition metal in the human body: the total cellular iron concentration is 0.3 ± 0.1 mM[92]. Under physiological conditions, iron exists in its stable redox states, ferrous ion (Fe^{2+}) and ferric ion (Fe^{3+}). The majority of cellular iron is tightly bound to enzymes and specialized transport and storage proteins[93], and labile iron is in a minor amount and bound loosely to anions, polyfunctional ligands *et al.*[94] Iron plays essential roles in various biological events, such as oxygen metabolism, electron transport, and DNA synthesis, which are based on its potent redox capacity[95]. On the other hand, iron overload causes severe cell damage and organ dysfunction through the abnormal production of reactive oxygen species (ROS)[96-97]. Furthermore, disruption of iron homeostasis has been linked to a number of disease processes such as cancer[98], hepatitis[99], and neurodegenerative diseases[100].

4.1 Fe(II) Sensors

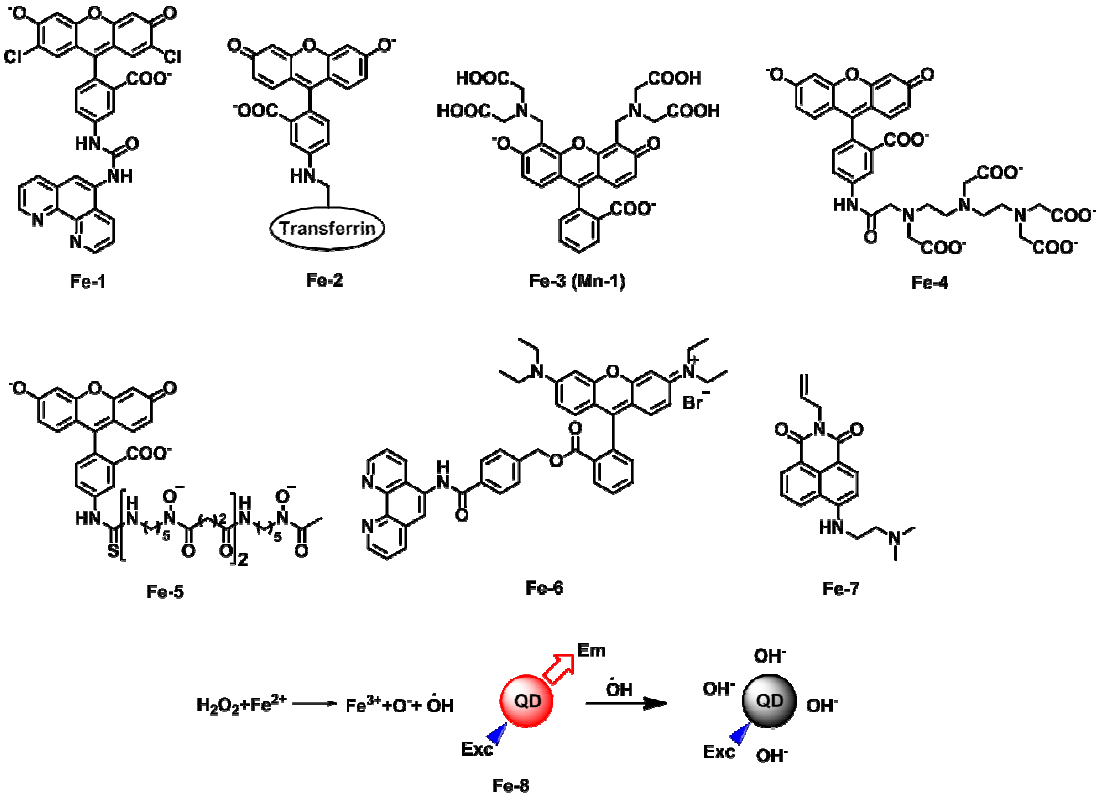

4.1.1 Fluorescent sensors for Fe(II)

"Turn-off" fluorescent sensors for Fe(II)

Cabantchik and co-workers[101-102] have reviewed a series of fluorescein (FL)-based Fe^{2+} sensors, in which the fluorescein fluorophore was coupled to highly specific iron chelators, transferrin, deferoxamine (DFO), ethylenediaminetetraacetic acid (EDTA), diethylenetriaminepentacetate acid (DTPA) or phenanthroline (phen). All of these fluorescent sensors underwent fluorescence quenching upon binding of iron, although they showed some variation in their iron-binding properties. The sensor: iron-binding stoichiometry was 1:1 for **Fe-3 (Mn-1)**, **Fe-4** and **Fe-5**, 1:2 for **Fe-2**, and 3:1 for **Fe-1**. The maximal quenching efficiency of the metal varied between 70 and 90%, depending on the sensor, with **Fe-1**, **Fe-3**, and **Fe-5** showing the highest values and negligible background, and **Fe-2** showing the lowest values with significant background signal. Fe^{2+} quenching of the FL-based sensors was found to follow an apparently mixed static and dynamic Stern-Volmer relationship, with linearity restricted to a relatively narrow range of quencher concentrations.

Fe-3 was employed to measure the labile iron pool (LIP) and the concentration of cellular free Fe^{2+}[103-107]. Cells are loaded with **Fe-3** *via* its acetomethoxy precursor, and then the ester group was hydrolysed by intracellular esterases. Strong iron chelators, such as salicylaldehyde isonicotinoyl hydrazone (SIH) and DFO, were used to regenerate the fluorescence of the **Fe-3**-Fe^{2+} complex. LIP was assessed from the relative rise in fluorescence intensity.

Similar to **Fe-3**, quantitative determination of LIP using **Fe-1**[108-110] is based on the fluorescence increased when cellular chelatable iron available to **Fe-1** was removed by the metal chelators, such as 2,2'-dipyridyl. Using fluorescence microscopy, Rauen and co-workers measured the LIP in isolated rat hepatocytes[108], single intact cells[109], and liver endothelial cells[110].

Rauen and co-worker[111] reported a fluorescent indicator (**Fe-6**) to determine mitochondrial chelatable ("redox-active") iron pool. In **Fe-6**, deprotonated rhodamine B was chosen for mitochondrial targeting and as a fluorophore, and phen as the iron-chelating component. The addition of Fe^{2+} strongly decreased the fluorescence intensity at 602 nm (λ_{ex} = 564 nm) of **Fe-6** in a "simple buffered solution" and a "mitochondrial medium". Besides Fe^{2+}, **Fe-6** fluorescence was markedly quenched by Cu^{2+}. **Fe-6** selectively accumulated in the mitochondria indicated by its co-localization with the mitochondria marker, rhodamine 123. The intramitochondrial fluorescence of **Fe-6** was quenched and increased upon addition of iron and the metal chelators pyridoxal isonicotinoyl hydrazone (PIH) and phen, respectively. Finally, the sensor was applied to the mitochondrial chelatable iron pool after inhibition of haem synthesis in hepatocytes and K562 cells.

A green fluorescent polyvinylcarbazole polymer with 1,8-naphthalimide side chains (**Fe-7**), reported by Grabchev *et al*[112], was demonstrated as a Fe^{2+} sensor. In DMF solution, the addition of Fe^{2+} leads to a decrease in the fluorescence intensity of the polymer system. The Fe^{2+} sensing property of **Fe-7** was also investigated in solid state, which has a similar behavior as in DMF solution. In addition, Yan and co-workers[113] developed a kinetic method based on glutathione capped CdTe quantum dots (QDs) (**Fe-8**) for discriminating Fe^{2+} and Fe^{3+}. Both Fe^{2+} and Fe^{3+} could quench the fluorescence of **Fe-8**, however the quenching kinetics was quite different for Fe^{2+} and Fe^{3+} resulting from the different electronic structures and redox potentials of metal ions. Trace H_2O_2 was introduced to establish a QDs-Fenton hybrid system for selective determination of Fe^{2+}. The Fenton reaction between Fe^{2+} and H_2O_2 resulted in hydroxyl radicals which effectively quench the fluorescence of the QDs through electron transfer from the conduction band of the QDs to the single occupied molecular orbit of hydroxyl radicals. The detection limit of this method for Fe^{2+} was 5 nM.

"Turn-on" fluorescent sensors for Fe(II)

On the basis of the tmeda-PPETE/Cu^{2+} hybrid system, Jones and co-workers[114] developed a "turn-on" fluorescence sensor (**Fe-9**) for Fe^{2+}. Cu^{2+} was preloaded onto tmeda-PPETE to quench the initial background fluorescence (quenched by more than 98%). A greater than 100-fold enhancement in the fluorescence intensity at 494 nm was observed upon titration of Fe^{2+} in THF, in which Fe^{2+} displaced Cu^{2+} from the receptor. The sensory system showed insignificant response toward the other cations, with the exception of Hg^{2+} (10-fold enhancement) and H^+ (21-fold enhancement). In another approach, Varma and co-workers[115] developed a dansyl-styrylquinoline conjugate (**Fe-10**) as a Fe^{2+}-selective sensor. The fluorescence spectrum of **Fe-10** in $CH_3CN–H_2O$ (9:1, v/v) showed very weak emission band centered at 450 nm, which was attributed by the ICT from quinoline nitrogen to nitrostyryl group upon excitation. On binding with Fe^{2+}, the ICT process was disrupted thereby and the fluorescence intensity was remarkably enhanced (15-fold).

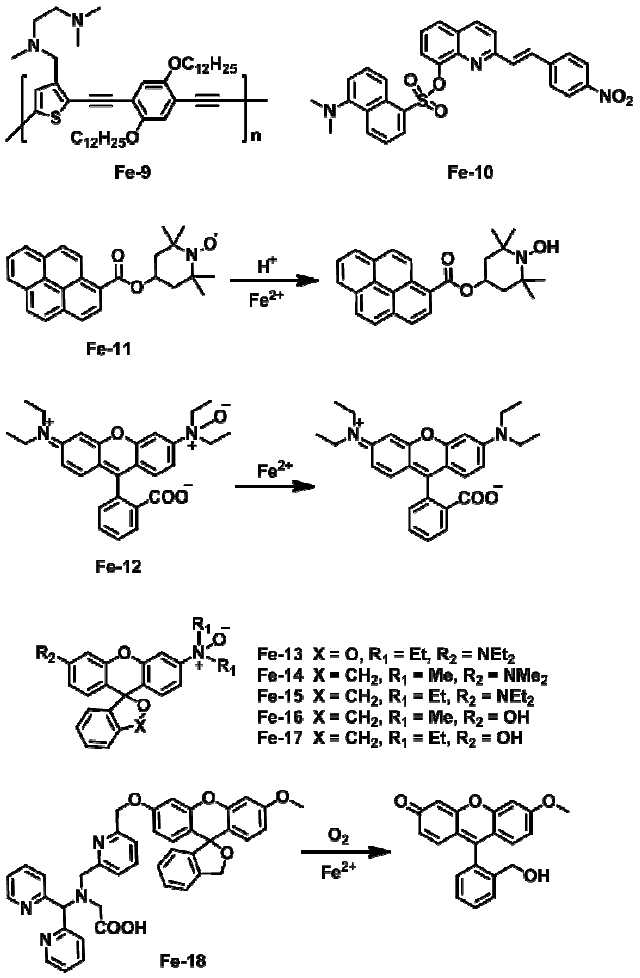

Zhu *et al*[116] developed a fluorescence method for the determination of Fe^{2+} based on specific redox reaction between spin fluorescence sensor pyrene-tetramethylpiperidinyl (**Fe-11**) and Fe^{2+}. The pyrene characteristic fluorescence of **Fe-11** was almost fully quenched, presumably owing to efficient intramolecular quenching of fluorophore by the nitroxide. The fluorescence intensity at 430 nm and the absorbance at 354 nm of **Fe-11** enhanced gradually with the addition of Fe^{2+}. The fluorescence enhancement is proportional to the concentration of Fe^{2+} in range of 2.4×10^{-7} to 3.6×10^{-6} M with a detection limit of 4.0×10^{-8} M. However, this reaction must be carried out in acidic solution. Another *N*-oxide chemistry based fluorescent sensor (**Fe-12**) for the selective detection of Fe^{2+} was developed by Nagasawa *et al*[96]. Fluorescence quenching (Φ = 0.010) of **Fe-12** occurred in a physiological buffer (50 mM HEPES buffer, pH 7.4), which was attributed to nonradiative deactivation of the excited state of tertiary amine *N*-oxide substituted xanthene involving a twisted internal charge transfer (TICT) process and partially due to PET from the *N*-oxide group. Upon addition of Fe^{2+}, the fluorescence intensity of the sensor increased by 30-fold *via* Fe^{2+}-mediated deoxygenation of the N-oxide group. **Fe-12** could visualize not only externally supplemented Fe^{2+} but also the endogenous labile Fe^{2+} in living cells. Co-staining experiments revealed that this sensor localized to the Golgi apparatus. Very recently, Nagasawa group[117] reported a series of Fe^{2+}-selective fluorescent sensors (**Fe-13**, **Fe-14**, **Fe-15**, **Fe-16**, **Fe-17**) based on the spirocyclization of hydroxymethylrhodamine and

hydroxymethylrhodol scaffolds. Compared with **Fe-12**, the spirocyclization strategy improved the "turn-on" rate dramatically and enhanced the reaction rate against Fe^{2+}. Finally, **Fe-14** was applied in monitoring the accumulation of labile iron in the lysosomes induced by transferring-mediated endocytosis.

Chang group[118] also reported a reaction-based Fe^{2+} fluorescent sensor that exploits a iron-mediated oxidative C-O bond cleavage reaction. **Fe-18** is weakly fluorescent in aqueous buffer (50 mM Tris, pH 7.6), and addition of Fe^{2+} leads to a 6-fold emission "turn-on" response within 1 h of reaction. Other cellular metal ions gave almost no response except Co^{2+}. **Fe-18** can detect changes in exchangeable iron stores within living cells upon iron supplementation or depletion, including labile iron pools at endogenous, basal levels. Co-staining experiments demonstrated that **Fe-18-AM** (**Fe-18** masked as an acetoxymethyl ester) localized to lysosomes. Moreover, **Fe-18** was used to identify reversible expansion of labile iron pools by stimulation with vitamin C or the iron regulatory hormone hepcidin.

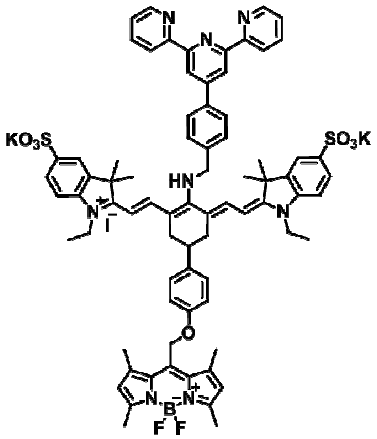

Fe-19

Ratiometric fluorescent sensors for Fe(II)

The first ratiometric Fe^{2+} fluorescent sensor (**Fe-19**) was reported by Tang *et al*[119]. 4'-(aminomethylphenyl)-2,2',6',2''-terpyridine (Tpy) was linked to a near-infrared fluorophore cyanine (Cy) as the Fe^{2+} responsive fragment, and BODIPY was harnessed as the insensitive fragment. When Fe^{2+} bound to the receptor-Tpy, an efficient PET process happened from the Fe^{2+}-Tpy complex to the Cy group. As a result, the fluorescence intensity of Cy-Tpy fragment (F_{635nm}) could be quenched instantaneously, whereas the fluorescence intensity of BODIPY fragment (F_{507nm}) was basically unchanged. The intensity ratio (F_{507nm}/F_{635nm}) showed a linear relationship toward the concentrations of Fe^{2+} (1.0×10^{-7} to 7.0×10^{-6} M) with a detection limit of 12 nM. Other competitive, biologically relevant metal ions did not interfere the fluorescence intensity ratio of **Fe-19**. Finally, this sensor was applied to fluorescence ratiometric imaging of Fe^{2+}, including adscititious and intracellular Fe^{2+} converted by ascorbic acid in live HL-7702 cells.

4.1.2 Colorimetric sensors for Fe(II)

Kim and co-workers[120] introduced a cap-type Schiff base **Fe-20** acting as a colorimetric sensor for Fe^{2+}, Cu^{2+}, and Zn^{2+} in HEPES–CH_3OH (99:1, v/v). **Fe-20** showed color changes from yellow to red in the presence of Fe^{2+} and from yellow to colorless in the presence of Cu^{2+} and Zn^{2+}. In the corresponding UV-vis spectra, a new absorption peak at 509 appeared for Fe^{3+} and the absorption peak at 400 nm decreased for Cu^{2+} and Zn^{2+}. Based on juloidine-imidazole moieties as binding and signalling unit, Kim *et al*[121] developed an optical receptor **Fe-21** for metal ions. **Fe-21** showed instantaneous color changes from colorless to orange and to purple in the presence of Fe^{2+} and Fe^{3+}, respectively. Meanwhile, the absorption peaks at 440 nm for Fe^{2+} and at 450 nm for Fe^{3+} increased in intensity. In another approach, the same group[122] developed a colorimetric sensor **Fe-22** for the detection of Fe^{2+} and Cu^{2+} in bis-tris–DMF (8:2, v/v, pH 7.0). The addition of Fe^{2+} and Cu^{2+} into **Fe-22** caused the significant spectral changes (new peaks at 455 nm for Fe^{2+} and 660 nm for Cu^{2+} appeared), which were accompanied with visual color changes from colorless to light orange and green, respectively.

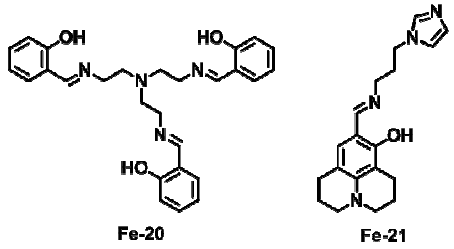

Fe-20 **Fe-21**

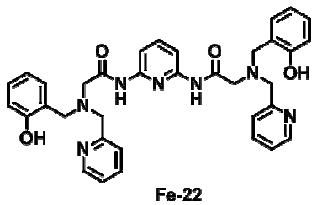

Fe-22

4.1.3 MRI contrast agents for Fe(II) sensing

The efficacy of a contrast agent is expressed by its relaxivity, r_1, defined as the longitudinal proton relaxation enhancement referred to 1 mM Gd^{3+} concentration. The factors contributing to the relaxivity value include the number of inner-sphere water molecules (q), the rotational tumbling time (τ_R), and the residence lifetime of inner-sphere water molecules (τ_m). The relaxivity of a responsive contrast agent is supposed to be selectively altered by the target analyte. Several self-assembly heterotrinuclear Gd(III)-Fe(II) complexes have been reported as MRI contrast agents. The ligand design was based on the combination of two different complexing moieties, each with structural characteristics for a preferential coordination mode[123]. The terpyridine[123-124], phenantroline[125-126], and bipyridine[127] units were employed to bind Fe^{2+}. On the other hand, DTTA[123, 127], DTPA[125], and DOTA[124, 126]-based ligands were used for Gd^{3+} complexing. These supramolecular assemblies were formed in the presence of Gd^{3+} and Fe^{2+}, resulting in a reduced rotational mobility and a relaxivity enhancement[4, 13]. Despite the fact that these agents were mainly studied as MRI contrast agents with high relaxivities, they could be potentially used as Fe^{2+}-responsive MRI sensors.

Merbach and co-workers[123] reported a trinuclear complex $[Fe(tpy\text{-}DTTA)_2Gd_2]$ (**Fe-23**) which has significantly increased relaxivity (r_1 = 17.4 mM^{-1} s^{-1} at 40 MHz, 37 °C), compared to the low molecular weight $[GdH(TTAHA)]^{2-}$ (r_1 = 7.3 $mM^{-1}s^{-1}$ at 20 MHz, 40 °C). **Fe-23** has a well-defined topology with favourable features to attain high relaxivities, *i.e.* a rigid $Fe^{2+}(tpy)_2$ core,

reduced flexibility at the periphery thanks to a short linker, and efficient separation of the two Gd^{3+} centres. The direct linkage of the polyaminocarboxylate moiety to the terpyridine part, although enchancing the rigidity, reduces the stability of the Gd^{3+} complex[14]. In addition, the $[Ru(tpy\text{-}DTTA)_2Gd_2]$ complex was also obtained, possessing a solution behavior similar to that of the iron complex[14].

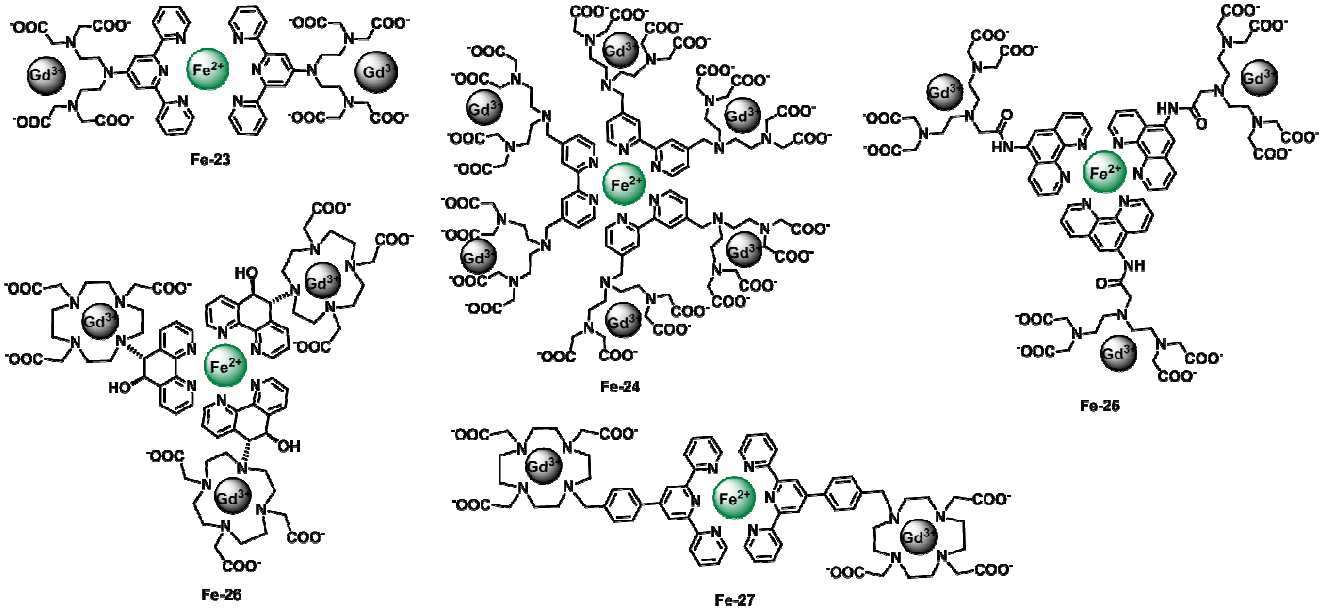

In another approach, Merbach *et al*[127] developed a bipyridine-based heterotritopic ligand which could self-assemble with Fe^{2+} and Gd^{3+} into a metallostar $\{Fe[Gd_2bpy(DTTA)_2]_3\}^{4-}$ (**Fe-24**) structure. A large increase in the relaxivity upon formation of **Fe-24** from $[Gd_2bpy(DTTA)_2]^{2-}$ (~100% at 30–60 MHz) was observed, and the molar relaxivity per Gd for **Fe-24** at 20 MHz and 37 °C was determined to be 20.17 $mM^{-1}s^{-1}$. Furthermore, MRI studies conducted at 4.7 T in mice confirmed that the metallostar displayed approximately four times higher *in vivo* relaxivity than the commercially available GdDOTA[128]. The pharmacokinetics of the metallostar was found to be similar to that of GdDOTA, involving fast renal clearance, a leakage to the extracellular space in the muscle tissue and no leakage to the brain. In addition, a high-molecular weight tetrametallic supramolecular complex $[Fe(Gd\text{-}DTPA\text{-}phen)_3]^-$ (**Fe-25**) was obtained upon self-assembly around one Fe^{2+} ion of three 1,10-phenantroline-based molecules by Parac-Vogt *et al*[125]. Compared to Gd-DTPA, **Fe-25** exhibited significant higher relaxivity (9.5 $s^{-1}mM^{-1}$) at 20 MHz and 37 °C, slower elimination from rats, reduced volume of distribution, and more organ accumulation according to the biodistribution profile.

Desreus and co-workers[126] prepared a ditopic ligand which exhibited the sought characteristics and was able to form a stable Gd^{3+} complex that easily self-assembles around Fe^{2+}. The alcohol group of the dihydro-phenanthroline unit remained coordinated to the encapsulated metal ion. Despite rather slow water-exchange rates, a 90% relaxivity increase was observed upon the formation of the heterometallic tris complexes (**Fe-26**) with high rigidity. Another DOTA-based ligand was reported by Chen *et al*[124]. This Gd_2Fe (**Fe-27**) array was prepared by incorporation of two Gd-containing units with a Fe^{2+} ion by self-assembly coordination. Relaxivity studies showed that **Fe-27** exhibited higher relaxation efficiency (r_1 = 7.56 $mM^{-1}s^{-1}$) compared to Gd-DTPA, arsing from the rigidity of the low-spin $Fe(tpy)_2$ unit.

4.2 Fe(III) Sensors

Similar to Cr^{3+}, the hydrolysis of Fe^{3+} is a fundamental process that occurs in neutral or alkaline conditions. The pH value of Fe^{3+}-containing (500 μM) water is around 3.47[23]. Therefore, no proton interference is also particularly important for the selective detection of Fe^{3+} in the aqueous solution.

4.2.1 Fluorescent Fe(III) sensors

"Turn-off" fluorescent sensors for Fe(III)

Shen group[129] developed two 2-(thiophen-2-yl)quinoline appended BODIPY sensors (**Fe-28** and **Fe-29**) for Fe^{3+}, with large Stokes' shift *via* TBET. Upon excitation of 5-(quinolin-2-yl)thiophen-2-yl at 334 nm, the fluorescence intensities from the BODIPYs of **Fe-28** at 532 nm and **Fe-29** at 732 nm decrease remarkably. The explanation for the fluorescence quenching is that the energy transfer from 2-(thiophen-2-yl)quinoline to the BODIPY is inhibited after binding with Fe^{3+}. Moreover, **Fe-28** can be used as a fluorescence "turn-off" sensor for Fe^{3+} in live MCF-7 cells. Cazier-Dennin and co-workers[130] reported a *N*-azacrown carbazole fluoroionophore **Fe-30** as a Fe^{3+}-selective sensor. The non-pH dependence of the fluorescence properties of **Fe-30** provides an effective mean for Fe^{3+} sensing in water. A 2,2'-bisbenzimidazole derivative **Fe-31**, reported by Wei and co-workers[131], displayed fluorescence quenching with high selectivity toward Fe^{3+} in DMSO–H_2O (6:4, v/v) solutions. Gao and co-workers[132] demonstrated a 8-hydroxyquinoline derivative **Fe-32** possessing a highly selective response of fluorescence quenching toward Fe^{3+} in DMF–H_2O (98:2, v/v) containing Britton-Robison buffer (10 mM, pH = 7.0). Wang and co-workers[133] have developed a dansyl-based Fe^{3+}-selective fluorescent sensor **Fe-33** with an electron-rich di-(2-picoly)amine (DPA) moiety as a receptor. In C_2H_5OH–H_2O (1:1, v/v) solution, the addition of Fe^{3+} ion caused the quenching effect on the fluorescence intensity of **Fe-33**, and the fluorescence of **Fe-33** is pH insensitive in the range from 3.0 to 11.0. A coumarin-derived

fluorescent sensor (**Fe-34**) for Fe^{3+}, developed by Guo *et al*[134], showed a decrease in the emission intensity at 448 nm upon treatment with Fe^{3+} in the Na_2HPO_4-citric acid buffer solution at pH 4.8. The sensor can be applied to the monitoring of Fe^{3+} with a pH span of 3.0–8.0. In addition, biological imaging, membrane permeability and nontoxicity demonstrate that **Fe-34** could act as a fluorescent sensor for Fe^{3+} in living cells. Very recently, Huo *et al*[135] have encapsulated a phenothiazine-derived shiff base in silica cross-linked micellar nanoparticles to build a water-soluble fluorescent sensor (**Fe-35**) for the selective detection of Fe^{3+} by fluorescence quenching through an electron transfer (ET) process.

Calix[4]arenes/thiacalix[4]arenes are one of the most actively studied molecular scaffolds used in molecular recognition of cations and anions[136]. Kumar *et al*[137-139] have developed a series of pyrene-appended sensors **Fe-36**, **Fe-37** and **Fe-38** for Fe^{3+} based on thiacalix[4]arene. The fluorescence spectrum of compound **Fe-36** gave strong monomer emission at 386 nm and there was no excimer emission band. Upon addition of Fe^{3+} ions to the solution of receptor **Fe-36**, a significant quenching in the fluorescence emission was observed which was attributed to paramagnetic nature of Fe^{3+} and reverse PET from pyrene units to the carbonyl oxygen of which the electron density was diminished upon metal ion complexation. Sensor **Fe-37** shows remarkably quenching of monomer and excimer emission bands in the presence of Fe^{3+} or Ag^{+}. In the case of sensor **Fe-38**, the addition of Fe^{3+} results in significant quenching in the excimer emission. Evaluation of the **Fe-38**-Fe^{3+} complex prepared in situ demonstrated the detection of Fe^{3+} in the presence of amino acids, blood serum and bovine serum albumin. Furthermore, compound **Fe-38** has suitable permeability into the PC3 cells and can be utilized as a Fe^{3+} sensor in living cells.

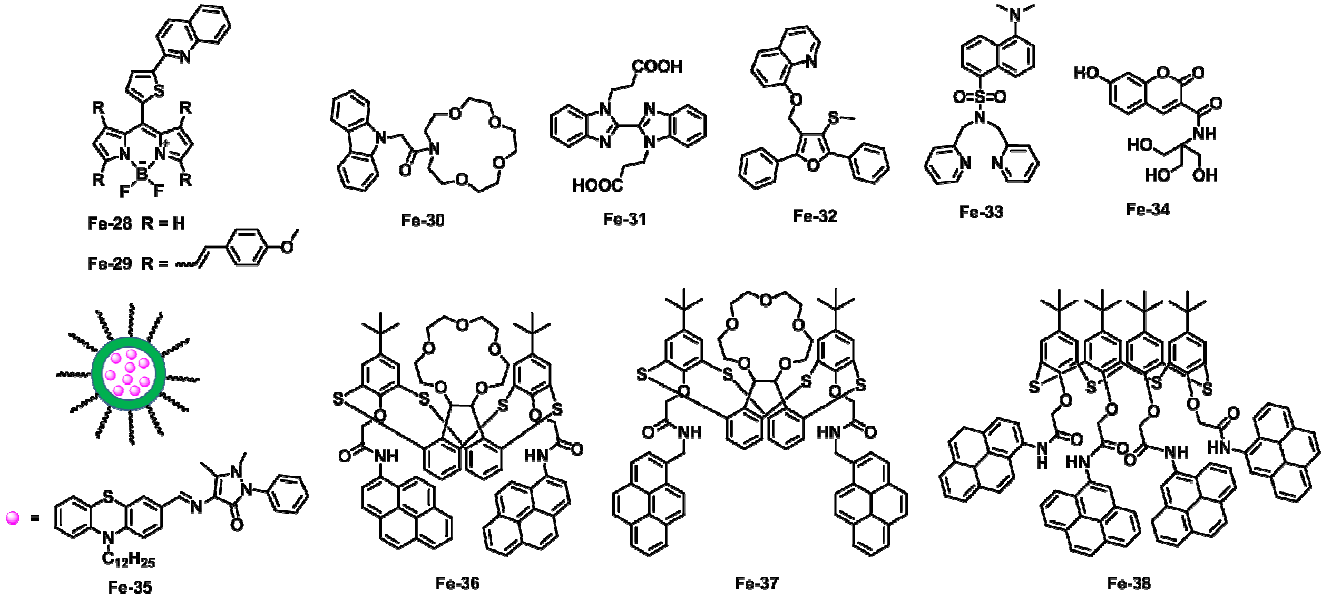

"Turn-on" fluorescent sensors for Fe(III)

Firstly, we introduce several examples of Fe^{3+}-selective fluorescent sensors based on rhodamine in recent years. Li and co-workers[140] reported a series of rhodamine-aminobenzothiazole conjugates as "turn-on" sensors (**Fe-39**, **Fe-40**, and **Fe-41**) for Fe^{3+}. No obvious absorption and fluorescence emission were observed in the absence of Fe^{3+} because the spirocyclic form of rhodamine prevailed. However, upon treating with Fe^{3+}, an intense absorption band centered at 558 nm, and concomitantly, a strong orange fluorescent emission band appeared at 580 nm, which was reasonably assigned to the delocalized xanthenes tautomer of the rhodamine group. Confocal laser scanning microscopy experiments have proven that these sensors could respond to the changes of Fe^{3+} concentrations in living cells.

Mandal and co-workers[141] designed a bis-rhodamine based sensor **Fe-42** which showed high selectivity to Fe^{3+}. The absorbance and fluorescence emission of **Fe-42** were highly enhanced upon injection of Fe^{3+} in CH_3CN–Tris-HCl (1:1, v/v, pH 7.4). Other competitive metal ions did not show any considerable influence except Cu^{2+} which showed a little interference. The pH titration experiment suggested that the spirolactam ring of **Fe-42** was stable above pH 4.0. Finally, sensor **Fe-42** was applied in the imaging of live fibroblast cells exposed to Fe^{3+}. In addition, the same group[142] developed another sensor **Fe-43** for the detection of Fe^{3+} by incorporating a triazole unit into a quinoline-rhodamine conjugate. Injection of equimolar concentrations of Fe^{3+} led to the development of a 744-fold intense absorption band with a maximum at ~530 nm and a 427-fold intense fluorescence emission band with a maximum at ~552 nm as compared to free **Fe-43**. The spirolactam ring of **Fe-43** was stable in the pH range 6.0–10.0. Moreover, sensor **Fe-43** could be used to image Fe^{3+} in live fibroblast cells and formulated into a polymeric thin film sensor for Fe^{3+} detection.

Zeng and co-workers[143] have developed a Fe^{3+}-selective fluorescent sensor **Fe-44** by binding a quinoline moiety to rhodamine 6G hydrazide. Upon addition of Fe^{3+} to **Fe-44** in C_2H_5OH–H_2O (3:7, v/v), significant enhancements in absorbance at 532 nm and fluorescence at 559 nm were observed. Bioimaging and micro computed tomography (MCT) studies demonstrated that **Fe-44** had good cell-membrane permeability and was applied in the detection of intracellular Fe^{3+}. Sensor **Fe-45** was synthesized by the condensation of rhodamine-B hydrazine and 2-(*N*-methylpiperazinylimino)acetaldehyde[144], which exhibited Fe^{3+}-selective enhancement in the fluorescence

at a pH range of 6.0–7.5. Tfouni and co-workers[145] reported a rhodamine-based sensor **Fe-46** for Fe^{3+} containing a salicyladehyde moiety. Biological assays with confocal microscopy showed the sensor could be used to image iron pools in B16-F10 cells. A bistriazole-appended rhodamine conjugate (**Fe-47**) reported by Liu group[146] displayed Fe^{3+}- and Cu^{2+}-selective dual channel fluorescence in $CH_3CN–H_2O$ (1:1, v/v, pH 7.8). Kumar and co-workers[147] have designed a bis-rhodamine based sensor **Fe-48** for the determination of Fe^{3+} in THF, with a detection limit of 1.1×10^{-9}M. As an alternative, sensor **Fe-49** containing two rhodamine fluorophores linked through a cystamine moiety acting as recognition site, was reported by Li *et al*[148]. The response behavior of **Fe-49** towards Fe^{3+} is pH independent in neutral condition (pH 6.0–8.0). The fluorescence imaging experiments demonstrated its practical application in Fe^{3+} imaging in living cells.

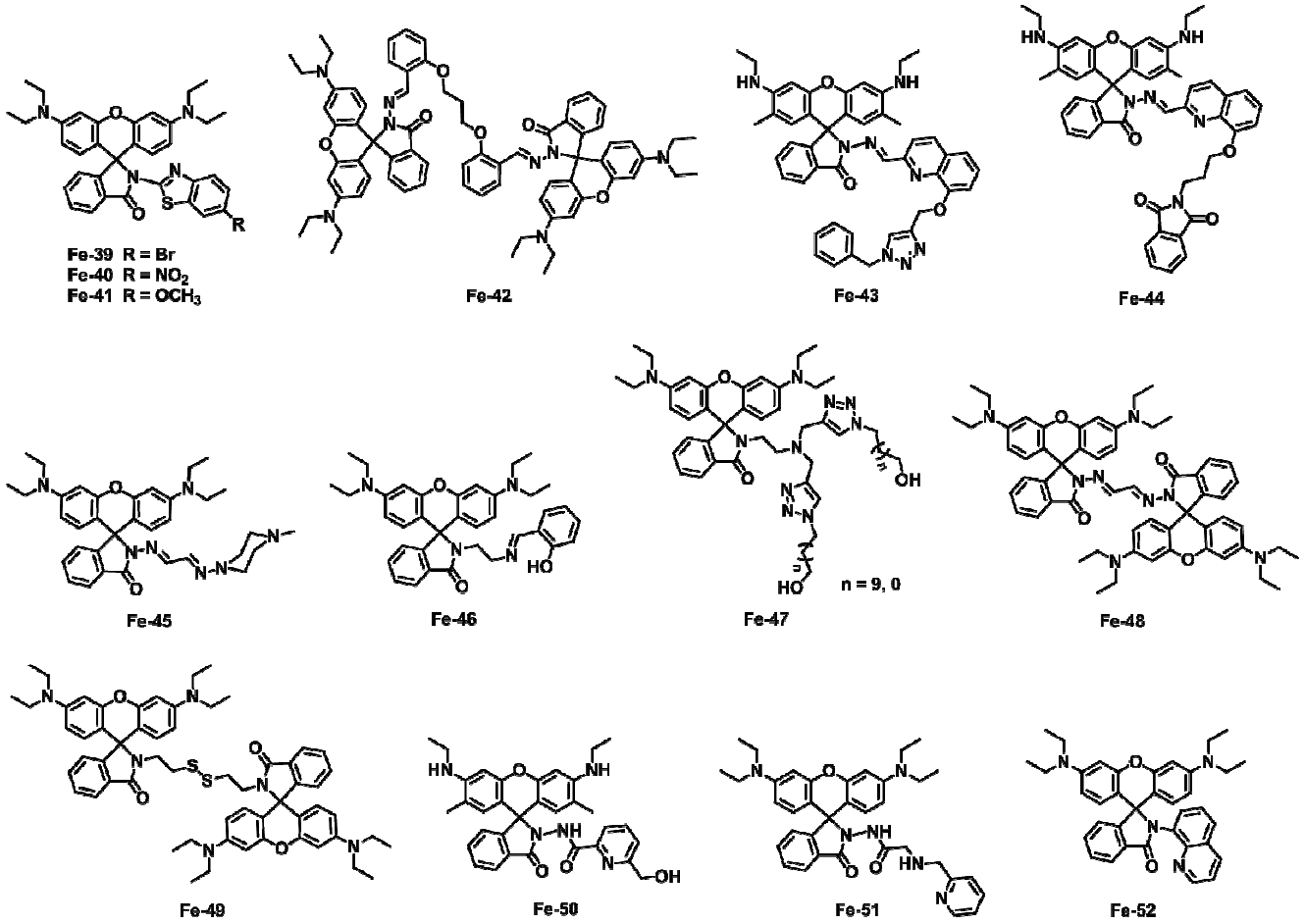

Goswami *et al*[149] demonstrated a rhodamine 6G-pyridine conjugate (**Fe-50**) as a Fe^{3+}-selective fluorogenic and colormetric sensor in $CH_3CN–H_2O$ (1:1, v/v, pH 7.2). The pH-emission plot showed insignificant changes in emission intensity of **Fe-50** in the pH range 7.0–10.5. **Fe-51**[150] is water-soluble "turn-on" fluorescent sensor for Fe^{3+} based on rhodamine B, in which the 2-picolylamine was chosen as the recognition group. **Fe-51** kept non-fluorescent in the pH range 6.0–9.0. The confocal fluorescence imaging indicated that **Fe-51** is cell permeable and can be used for monitoring intracellular Fe^{3+}. By integrating rigid 8-aminoquinoline moiety to rhodamine chromophore, Qian group[151] reported a fluorescent sensor for Fe^{3+} (**Fe-52**) in HEPES buffer solution (20 mM, pH 6.95) contained 50% CH_3CN as the cosolvent. Cu^{2+} and Cr^{3+} induced a mild response, while other metal ions had minor interference. The acid-base titration experiments revealed that **Fe-52** was insensitive to pH in the range from 6.0 to 12.0. The live cell imaging experiments demonstrated that **Fe-52** was cell-compatible and would serve as a Fe^{3+}-responsive bioimaging sensor.

Besides the rhodamine-based sensors, a few more examples have also been developed recently. Schiff bases with a bridged C=N structure easily isomerize in the excited state which usually results in weak fluorescence of the attached fluorophore. But when they form complexes with some special metal ions, the C=N isomerisation is inhibited and fluorescence enhancement can be achieved. Wang *et al*[152] reported a coumarin Schiff base compound (**Fe-53**) evaluated as a "turn-on" Fe^{3+} and Al^{3+} sensor. **Fe-53** showed weak fluorescence signal in MeOH, whereas significant enhancements of fluorescence at 488 nm and 516 nm were present with addition of Fe^{3+}/Al^{3+}. Li and co-worker[153] designed a carbazole-based Schiff base (**Fe-54**) behaving as a fluorescent sensor for Fe^{3+} and Cu^{2+}. In CH_3CN solution, **Fe-54** exhibited weak fluorescence at 423 nm and a dramatic enhancement was observed in the presence of Cu^{2+}/Fe^{3+}. A coumarin-naphthalimide conjugate (**Fe-55**) with Schiff base as bridge reported by Ren and co-workers[154] was used for the selective detection of Fe^{3+}. Upon addition of Fe^{3+} ion to the THF–H_2O (1:1, v/v) solution of **Fe-55**, a remarkable

enhancement of emission intensity was observed at 504 nm.

Hydroxylamine can be easily oxidized by Fe^{3+} while other metal ions have almost no interference. Chen and co-workers[155] used this reaction to develop a Fe^{3+}-selective "turn-on" fluorescent sensor (**Fe-56**). In the HEPES aqueous buffer (pH 7.40, 40 mM), the fluorescence intensity (λ_{em} = 615 nm) increased significantly upon the addition of Fe^{3+}, indicating that the PET process is regulated in the molecule. The fluorescence profiles of **Fe-56** were unchanged in the presence of other metal ions tested except Cu^{2+} which gave a limit enhancement at higher concentration. Confocal microscopy images established that **Fe-56** could respond to intracellular Fe^{3+} level. Another PET-based sensor **Fe-57**[156], synthesized by linking three 1,8-naphthalimide fluorophores with a tris(aminoehylamine) ligand, displayed high selectivity to Fe^{3+}. In DMF–H_2O (2:3, v/v) solution, Fe^{3+} caused an outstanding enhancement in fluorescence intensity at 493 nm of **Fe-57**. However, the pH titration experiment indicated that the Fe^{3+}-sensing behavior of **Fe-57** is available only in acidic medium.

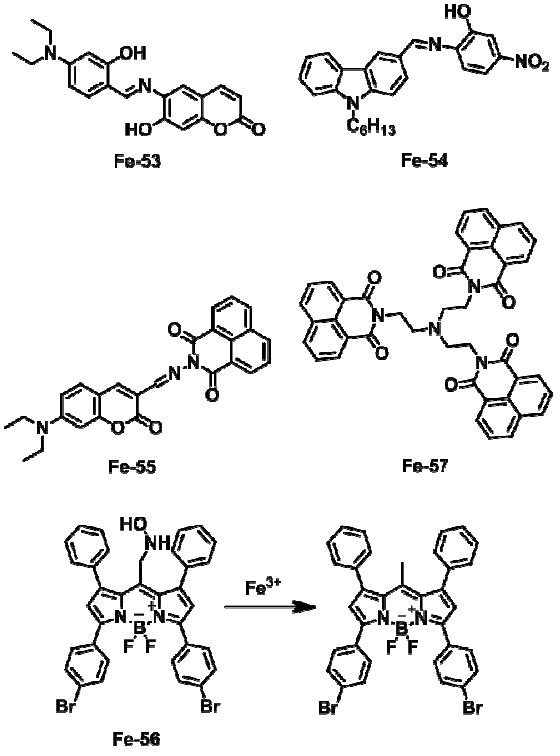

Ratiometric fluorescent sensors for Fe(III)

Chattopadhyay and co-workers[157] designed a ratiometric fluorescent sensor **Fe-58** which can discriminate between the two oxidation states (II/III) of iron depending on the pH of the medium. **Fe-58** undergoes a solvent assisted 1,5-σ tropic shift leading to a benzimidazole derivative (**Fe-58'**). In the CH_3CN–HEPES buffer (1:4, v/v, pH 4.5) solution of **Fe-58'**, addition of Fe^{2+} caused a decrease in fluorescence at 412 nm and an increase in fluorescence at 472 nm due to the formation of mononuclear Fe^{2+} complex. However, a decrease at 412 nm and an increase at 482 nm were observed during titration of Fe^{3+} to **Fe-58'** solution at pH 7.4 due to the formation of binary Fe^{3+} complex. Moreover, the sensor is efficient for detecting Fe^{3+} *in vitro* by developing fluorescence images of living cells. A polyphenyl derivative **Fe-59** developed by Li *et al*[158] exhibited a Fe^{3+}-selective ratiometric fluorescent signalling behavior. Upon addition of Fe^{3+} to the solution of **Fe-59** in C_2H_5OH–H_2O (10:1, v/v), a new fluorescence emission peak at about 455 nm appeared and the intensity dramatically enhanced with that at 361 nm decreasing. The red-shift and enhancement of the emission can be ascribed to the reformed orbital and the inhibition of the rotation of C–C bonds between each two aromatic rings, respectively. Liu and co-workers[159] reported a benzothiazole derivative **Fe-60** which behaves as a Fe^{3+}-selective fluorescent sensor in CH_3CN. Upon binding with Fe^{3+}, the emission band of **Fe-60** red-shifted from 370 nm to 420 nm and the fluorescence intensity was enhanced ~103-fold. The lowest Fe^{3+} concentration detected by **Fe-60** was down to 6.04×10^{-8} M. These results were mainly caused by CHEF mechanism. In mixed solvent (CH_3CN–H_2O, 98:2, v/v), the fluorescence enhancement of **Fe-60** caused by Fe^{3+} was much lower than that in pure CH_3CN.

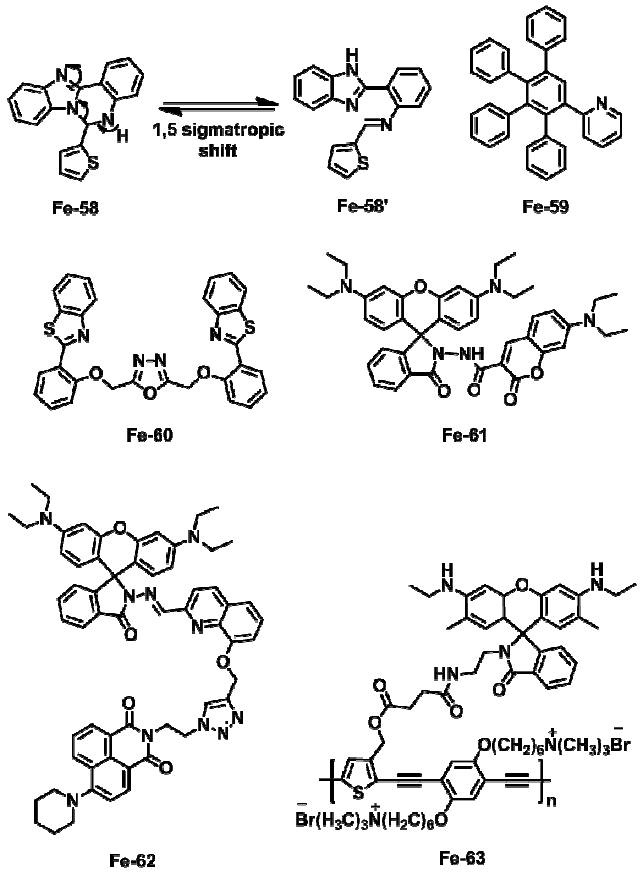

Next, we discussed some FRET-based ratiometric Fe^{3+} sensors. Zhao group[160] designed a coumarin-rhodamine system **Fe-61**. In C_2H_5OH–HEPES (99:1, v/v, pH 7.2), **Fe-61** showed an emission at 460 nm attributed to the coumarin moiety. Upon addition of Fe^{3+}, the peak at 460 nm increased slightly, and a new fluorescence peak appeared at 580 nm attributed to rhodamine B part. The Fe^{3+}-sensitive behavior of **Fe-61** is due to the ring-opening process of the rhodamine B unit along with the PET process suppressed simultaneously. **Fe-61** did not give obvious response for other metal ions except Cu^{2+} and Ni^{2+} which induced some fluorescence quenching. Sensor **Fe-62** reported by Thennarasu and co-worker[161] was used for the selective

ratiometric detection of Fe^{3+}. The triazole appended quinoline-rhodamine conjugate acts as an ionophore as well as the FRET energy acceptor and 8-piperzaino naphthalimide moiety as the donor. Upon addition of Fe^{3+} ions to sensor **Fe-62** in a CH_3CN–Tris-HCl (1:1, v/v, pH 7.4) buffer solution, the emission at ~532 nm decreased and a new emission band centered at ~580 nm appeared. The detection limit calculated using the emission at 532 nm was ~5.0×10^{-8} M. The spirocyclic form of **Fe-62** was stable in the pH range 5.0–10.0. The fluorescence microscopic experiments demonstrated the ability of sensor **Fe-62** in ratiometric monitoring intracellular Fe^{3+} ions. By combining a rhodamine spirolactam with a water-soluble ionic conjugated polymer (CP), Tan and co-workers[162] designed a FRET-based ratiometric sensing platform (**Fe-63**) for Fe^{3+}. In Tris-HCl (pH = 7.2) buffer solution, the introduction of Fe^{3+} induced a clear see-saw-type dual-emission change, suggesting the recovery of FRET from the CP backbones (donor) (I_{max} 442 nm) to the rhodamine 6G (I_{max} 538 nm). The good response of **Fe-63** toward Fe^{3+} was observed in the neutral pH range (7.0–8.0). Finally, this sensor was applied to ratiometric imaging of Fe^{3+} in HeLa cells.

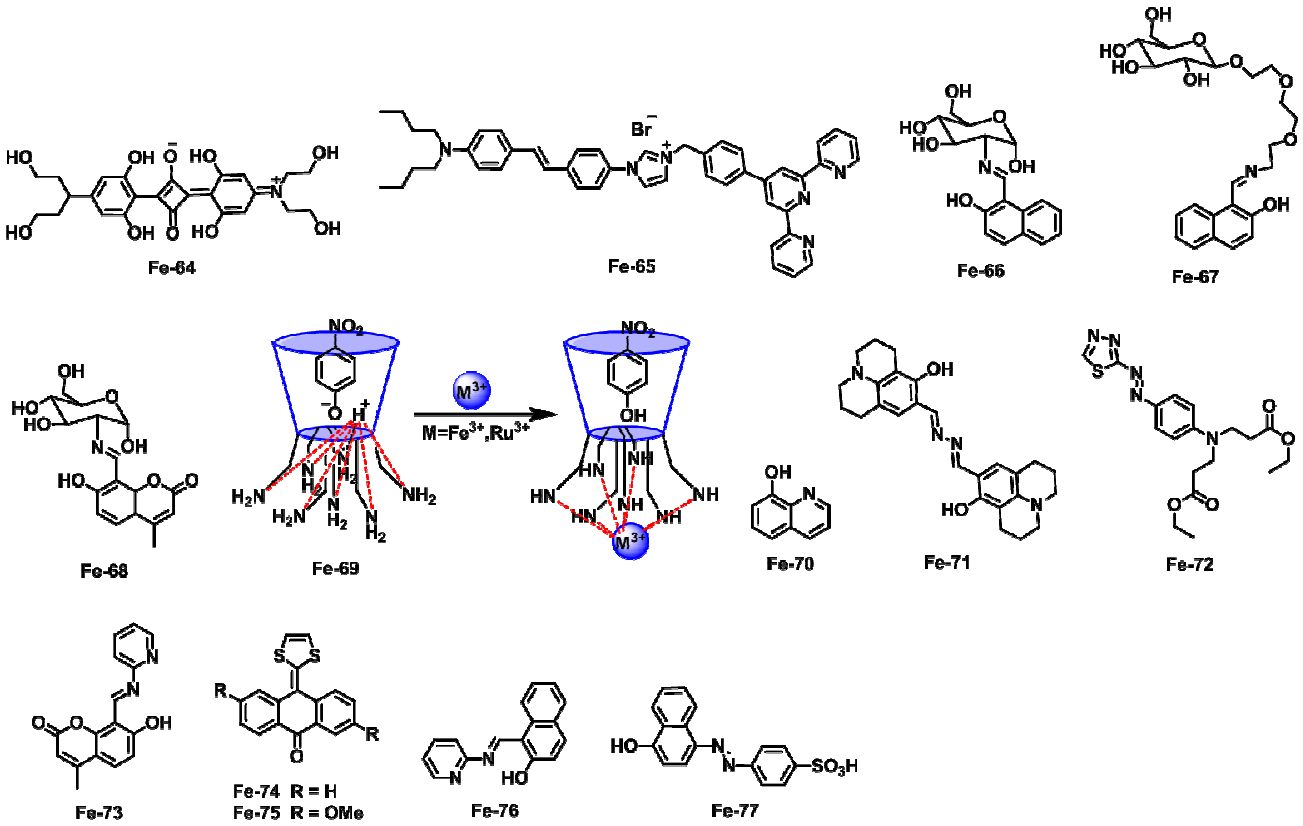

4.2.2 Colorimetric sensors for Fe(III)

Anslyn and co-workers[163] developed an artificial siderophore in the form of a squaraine dye (**Fe-64**) which acted as a Fe^{3+}-selective chelator. On the addition of Fe^{3+} to a DMSO solution of **Fe-64** containing one equivalent of 1,8-diazobicyclo[5.4.0]undec-7-ene (DBU), a decrease in absorbance intensity at 555 nm with an increase at 651 nm through a pseudo-isobestic point at 580 nm was observed, which was due to a subtle geometry change of **Fe-64** on chelation to Fe^{3+}. However, the optical response was seen to a lesser extent for the other metals, with the exception of Zn^{2+}. Interestingly, another band at 970 nm appeared in the UV-Vis-NIR spectrum for all of the metal titrations, which was good evidence that squaraine **Fe-64** was chelating to the metal ions, and that the metal-to-ligand-charge-transfer (MLCT) phenomenon was responsible for the hyperchromic shift observed. Sensor **Fe-65**, containing terpyridine for the selective detection of Fe^{2+} and Fe^{3+}, was reported by Yang and co-workers[164]. Upon the addition of Fe^{2+} or Fe^{3+} in aqueous solution at pH 6, the sensor displayed a unique new peak around 567 nm in its absorption spectra, and the color of the solution changed from light yellow to light magenta, which was caused by MLCT. In contrast, other metal ions did not produce significant changes in the UV-vis spectra at 567 nm, except that Ag^{+} induced a new band at 450 nm.

Rao and co-workers[165] reported a glucose-based C2-derivatived colorimetric sensor (**Fe-66**) for the recognition of Fe^{2+} and Fe^{3+}. Among the metal ions studied, only the Fe^{2+} or Fe^{3+} ions gave distinct visual color changes in an aqueous HEPES buffer (pH 7.2). In the absorption spectra, the changes observed with 300, 420 and 550 nm bands were suggestive of the metal ion complex formation. Inspired by their work, Du and co-workers[166] designed another two sugar-functionalized Fe^{3+}-selective colorimetric sensors (**Fe-67** and **Fe-68**). Both **Fe-67** and **Fe-68** had good solubility in pure water and high selectivity toward Fe^{3+}. Addition of other cations, including Fe^{2+} caused no detectable color changes to the naked eye.

Using per-6-amino-β-cyclodextrin (**B**) as a supramolecular host and *p*-nitrophenol (**C**) as a spectroscopic probe, Pitchumani and co-workers[167] developed a colorimetric method for Fe^{3+} and Ru^{3+} in water. When **C** formed a complex with **B**, the phenolic proton of **C** is abstracted by the amino groups of **B** resulting in intense yellow colour (λ_{max} 402 nm). Upon addition of Fe^{3+} or

Ru^{3+} to a solution of **Fe-69** in water, the absorbance at 402 nm decreased significantly with the emergence of a band at 318 nm, accompanied by a color change from intense yellow to colorless. This phenomenon could be explained by that complexation of metal ions with the amino groups of **Fe-69** resulted in simultaneous back transfer of the proton from **Fe-69** to *p*-nitrophenolate anion regenerating the colorless CD-*p*-nitrophenol complex.

Okoro and co-workers[168] have developed a spectrophotometric method for the determination of Fe^{3+} using 8-hydroxyquinoline as a chromogenic reagent (**Fe-70**). The proposed method was based on the reaction of Fe^{3+} with **Fe-70** in chloroform solution to form a metal-oxine complex having a maximum absorption at 359 nm. The method gave good recovery and the determination of Fe^{3+} using the method was accurate as the sophisticated AAS. In another approach, an aldazine-based colorimetric sensor **Fe-71** for Fe^{3+} was reported by Govindaraju and co-workers[169]. Addition of Fe^{3+} led to a change in the color of **Fe-71** solution from pale yellow to violet and absorption band at 445 nm red-shifted to 575 nm, which was due to deprotonation of phenolic–OH which allowed the charge transfer from ligand to metal ions. There was no significant change in the absorption band of **Fe-71** in the presence of various other metal ions tested except Al^{3+} which induced a slightly red shift.

Kaur *et al*[170] described a pH stable hetarylazo dye (**Fe-72**) equipped with binding sites consisting of N, S and N, O combinations which showed selectivity towards Hg^{2+} and Fe^{3+}. In the titrations of Hg^{2+} or Fe^{3+} with **Fe-72** in CH_3CN, a decrease in the intensity of the absorption band of **Fe-72** at 480 nm was attended by appearance of the twin absorption bands at 531 and 564 nm. Meanwhile, distinct naked-eye color changes for Hg^{2+} (yellow to purple) and Fe^{3+} (yellow to red) were observed. Yen and co-workers[171] introduced a coumarin derivative **Fe-73** possessing dual sensing ability for Fe^{3+} and Mg^{2+}. The sensor exhibited selective and sensitive recognition towards Fe^{3+} in CH_3CN *via* color change from colorless to brown. In the UV-vis spectra, the addition of Fe^{3+} caused an increase in absorbance at 280, 298, 345 nm and appearance of a new absorption peak at 538 nm. Also it showed a significant fluorescence enhancement (70-fold) towards Mg^{2+} in $CH_3CN–H_2O$ (8:2, v/v) solution.

Chen and co-workers[172] reported two push-pull molecules **Fe-74** and **Fe-75** containing a donor 1,3-dithiole ring and an acceptor carbonyl group behaving as a colorimetric sensor for the detection of Fe^{3+} and Cu^{2+}. The orange solution of **Fe-74** or **Fe-75** was bleached completely to colorless after the addition of Cu^{2+} and Fe^{3+}. In the corresponding UV-vis spectra, a dramatic decrease of the absorption band at 467 nm was observed. The NMR spectra and EI mass illuminated that the sensing mechanism of **Fe-74** and **Fe-75** was that the oxidative activation of Cu^{2+} and Fe^{3+} induced the breaking of the double bond between the anthraquinone moiety and the 1, 3-dithiole ring, destroying the conjugated system and consequently leading to the color changes.

Sensor **Fe-76**, bearing naphthol O–H and imine group and reported by Zhang and co-workers[173] showed both colorimetric detection for Fe^{3+} and fluorescence "turn-on" response for Zn^{2+}. When Fe^{3+} was added to the DMSO solution of **Fe-76**, a dramatic color change from yellow to colorless was observed. In the corresponding UV-vis spectrum, a strong and broad absorption band from 413 to 480 nm disappeared. On the other hand, it led to a prominent fluorescence enhancement at 483 nm upon the addition of Zn^{2+} to **Fe-76**. Sensor **Fe-77** was developed by Yan and co-workers[174] for colorimetric determination of Fe^{3+} from brick-red to light red in aqueous solution at pH 7.0. Meanwhile, a decrease in the absorption intensity at 478 nm was observed, Under the optimum conditions, the detection possessed a linear range of 9.5 to 400 × 10^{-8} M and a detection limit of 4.2 × 10^{-9} M.

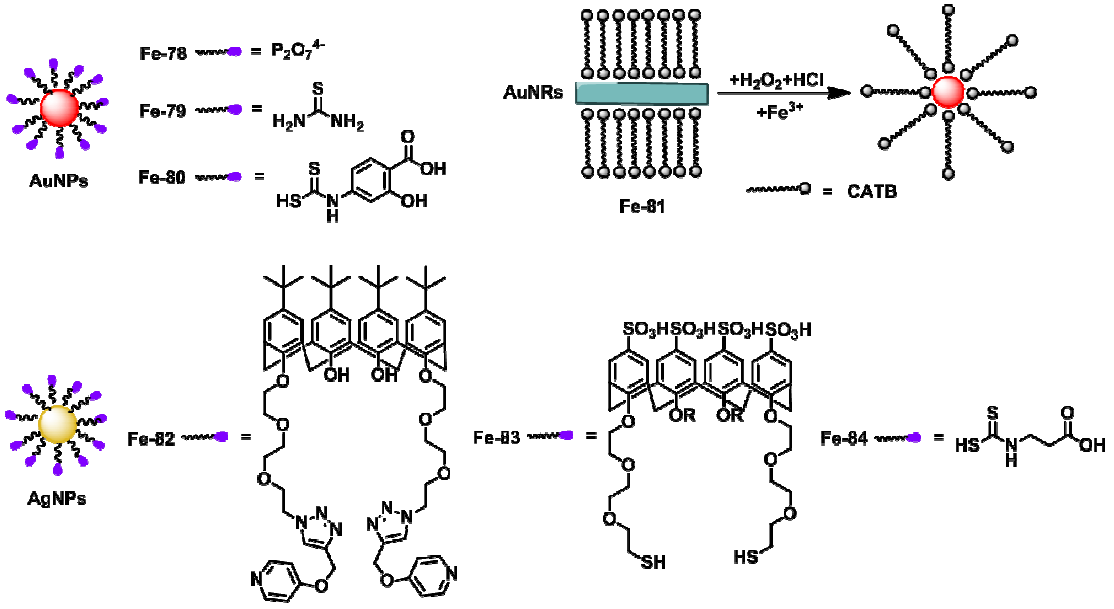

Next, a few examples of colorimetric Fe^{3+} sensors based on AuNPs will be discussed. Wu *et al*[175] have introduced a selective colorimetric Fe^{3+} detection method using pyrophosphate ($P_2O_7^{4-}$) functionalized AuNPs (**Fe-78**). The absorbance of **Fe-78** at 535 nm decreased with increasing Fe^{3+} concentration, accompanied by the formation of a new band at 750 nm as a result of the induced aggregation of AuNPs. Kailasa and co-workers[176] developed *p*-amino salicylic acid dithiocarbamate functionalized

AuNPs (**Fe-79**) as colorimetric sensors for Fe^{3+}. **Fe-79** was aggregated rapidly by addition of Fe^{3+} ions, yielding a color change from red to blue. In the corresponding UV-vis spectral, the characteristic SPR peak (520 nm) was shifted to 700 nm. In addition, a colorimetric, label-free, and non-aggregation-based AuNP sensor (**Fe-80**) for the highly selective detection of Fe^{3+} was reported by Han and co-workers[177]. UV-vis spectroscopy of an aqueous dispersion of AuNPs in the presence of HCl and thiourea yielded a distinct surface plasmon (SP) absorbance peak at 525 nm. The addition of Fe^{3+} ions caused the absorbance peak to sharply decrease in intensity, which was attributed to the Fe^{3+}-catalyzed leaching of AuNPs in the acidic thiourea system.

Different from AuNPs, gold nanorods (AuNRs) possess two plasmon absorption bands: longitudinal plasmon absorption band (LPAB) and transverse plasmon absorption band (TPAB). Liu *et al*[178] developed a non-aggregation colorimetric sensor (**Fe-81**) for the determination of Fe^{3+} based on the signal amplification effect of catalyzing H_2O_2 to oxidize AuNRs. The initial AuNRs exhibited two Plasmon absorption bands located at 716 nm for LPAB and at 520 nm for TPAB, respectively. When Fe^{3+} was added in the AuNRs-H_2O_2-HCl system, the blueshift of LPAB was observed with decrease of the corresponding absorbance, resulting in that plasmon absorption bands located at 558 nm for TPAB. The phenomenon could be explained as Fe^{3+} had strong catalytic effect on the oxidation reaction between H_2O_2 and AuNRs, leading to the changes in the gold nanostructures from rods to spheres.

Compared with AuNPs, AgNPs are much less stable due to the chemical degradation of AgNPs under the functionalization conditions and the exposure of the silver surface to oxidation[179]. However, the benefit of using AgNPs rather than AuNPs is that the molar extinction coefficient is 100-fold greater, which increases sensitivity and leads to improved visibility. Li and co-workers[180] employed a pyridyl-appended calyx[4]arene to modify AgNPs with a distinct colorimetric response to Fe^{3+}. Free **Fe-82** in solution showed one major absorption band centered at 414 nm. Among various metal ions, only Fe^{3+} ions induced the anticipated color change from yellow to colorless, corresponding to an absorbance peak at 364 nm, which was attributed to the Fe^{3+}-induced aggregation of AgNPs. In a similar approach, Menon and co-workers[181] reported a highly selective and ultrasensitive calyx[4]arene modified silver nanosensor (**Fe-83**) for Fe^{3+} recognition. The color of **Fe-83** was vivid yellow and displayed a characteristic absorption band at 422 nm. However, a color change to pale red and the appearance of a new band at 554 nm took place due to the aggregation of AgNPs in the presence of Fe^{3+}. The linear range for Fe^{3+} using **Fe-83** was found to be 10–100 nM, and the detection limit was 9.4 nM. In addition, Sahoo and co-workers[182] have developed a nanosensing system (**Fe-84**) by the surface functionalization of AgNPs with *β*-alanine dithiocarbamate for the selective recognition and monitoring of Hg^{2+} and Fe^{3+} ions. Addition of Hg^{2+} and Fe^{3+} to **Fe-84** solution resulted in the instantaneous decoloration accompanying the disappearance of the SPR absorption maxima at 402 nm. However, the addition of other metals showed no obvious color or spectral changes except Al^{3+} which resulted in a slight red shift in the SPR band of AgNPs. The DLS analyses suggested the aggregation of AgNPs upon addition of Hg^{2+} and Fe^{3+}.

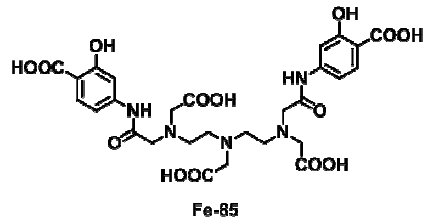

Fe-85

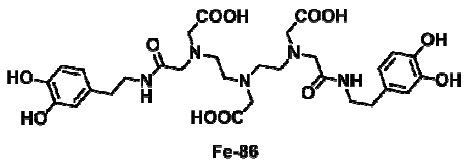

Fe-86

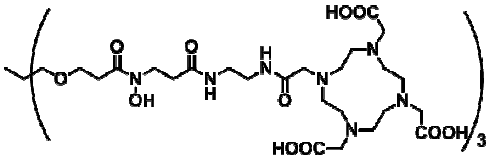

Fe-87

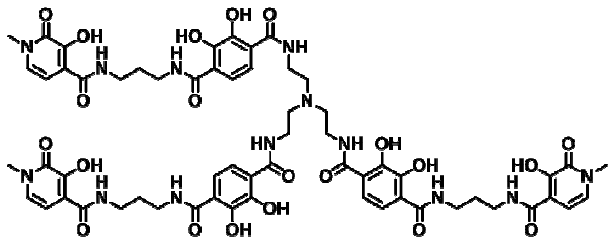

Fe-88

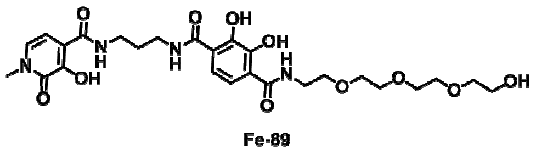

Fe-89

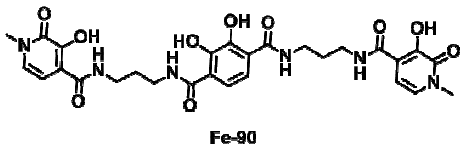

Fe-90

4.2.3 MRI contrast agents for Fe(III) sensing

Aime *et al*[183] have developed a DTPA-bis-salicylamide based ligand [DTPA(PAS)$_2$] (**Fe-85**), able to form stable heterobimetallic complexes with Gd^{3+} and Fe^{3+} ions. The Gd-Fe complex ([Gd-DTPA(PAS)$_2$]$_2$Fe or [Gd-DTPA(PAS)$_2$]$_3$Fe depending on the pH of the aqueous solution) exhibited a slight increased relaxivity respect to the precursor complex [Gd-DTPA(PAS)$_2$]$^{2-}$ (from 4.6 to 5.7 $mM^{-1}s^{-1}$ at 25 °C and 20 MHz), which might be ascribed to the increased molecular size of the complex. In a similar approach, Parac-Vogt *et al*[184] reported a

DTPA-bis(3-hydroxytyramide) [DTPA(HTA)$_2$] ligand (**Fe-86**) for complexing with Gd^{3+} and Fe^{3+}. Special attention was paid to avoid the formation of polymeric species by using tripodal nitrilotriacetic acid (NTA) ligand. A tris-hydroxamate ligand (**Fe-87**) was exploited to complex with Fe^{3+} in another Fe^{3+}-sensitive MRI contrast agent[185]. The Fe^{3+} chelation restricted free rotation at the Gd^{3+} center, thereby increasing the relaxivity of the contrast agent (from 5.4 to 8.5 $mM^{-1}s^{-1}$ at 20 MHz) without changing its molecular weight. In addition, Raymond and co-workers[186] developed a series of bis-bidentate ligands (**Fe-88**, **Fe-89**, and **Fe-90**) designed comprising two different binding sites, hydroxypridinone-based ligand HOPO selective for Gd^{3+} and terephthalamide-baed ligand TAM for Fe^{3+}. Relaxivity studies indicated that the high-molecular-weight clusters effectively slowed the molecular tumbling. This and the fast water exchange produce high relaxivity at the high magnetic fields (the relaxivity of [Gd_2(**Fe-80**)$_3$Fe)] is r_{1p} = 21 $mM^{-1}s^{-1}$ per Gd(III) at 90 MHz).

5. Cobalt

Cobalt is an essential trace element in both prokaryotes and eukaryotes. Cobalt occurs less frequently in metalloproteins than other transition metals due to its low abundance in nature as well as competition with iron[187]. Generally, biological cobalt is used as a cofactor in the corrinoid form. For example, cobalt is a core component of vitamin B12 which is involved in DNA synthesis, formation of red blood cells and maintenance of the nervous system[187-189]. However, unregulated cobalt is toxic to cells: the deficiency leads to anemia, retarded growth, loss of appetite and is one of the main risk factors for cardiovascular diseases[190-191]; excess dose causes diarrhea, giddiness cardiomyopathy, hyperglycemia, cancer and so on[191], the maximum tolerable level of Co is *ca.* 10 ppm[192].

5.1 Fluorescent sensors for Cobalt

"Turn-off" fluorescent sensors for Cobalt

Zamochnick and Rechnitz[193] developed a fluorescence extinction method for the determination of Co^{2+} in the ppb range, which is based on the reaction between Co^{2+} and the fluorescent aluminium-Superchrome Blue Black Extra (**Co-1**) complex. The fluorescence intensity of the complex decreases sharply in the presence of Co^{2+}, the decrease being linear over a concentration range of 0.001 μg to 0.02 μg per ml of final solution. Although the method exhibited high sensitivity and reproducibility (the average error is 1.29% when reading the fluorescent intensities from the potentionmetric recorder), the selectivity could be improved further (Cr^{3+}, Cu^{2+}, Ni^{2+}, Fe^{3+}, Al^{3+} and Cd^{2+} all showed some interference).

Monteil-Rivera[194] studied the fluorescence quenching of a Leonardite humic acid (LHA) by Co^{2+} at different pH. The interaction was monitored by emission fluorescence and by synchronous fluorescence with two different offsets ($\Delta\lambda_1$ = 20 nm and $\Delta\lambda_2$ = 80 nm). It was found that synchronous fluorescence performed with $\Delta\lambda_1$ resolves the individual components of the heterogeneous material better than emission or synchronous fluorescence performed with $\Delta\lambda_2$; however, it gives rise to fluctuating values rather than steadily decreasing values as expected for pure quenching curves. The quenching profiles obtained for pH 5.0, 6.0, and 7.0 by emission and synchronous ($\Delta\lambda_2$) fluorescence were analyzed by two methods: 1. a non-linear least-squares procedure first proposed by Weber *et al*[195-196]; and 2. a pH-dependent discrete logK spectrum model initially introduced by Westall *et al*[197].

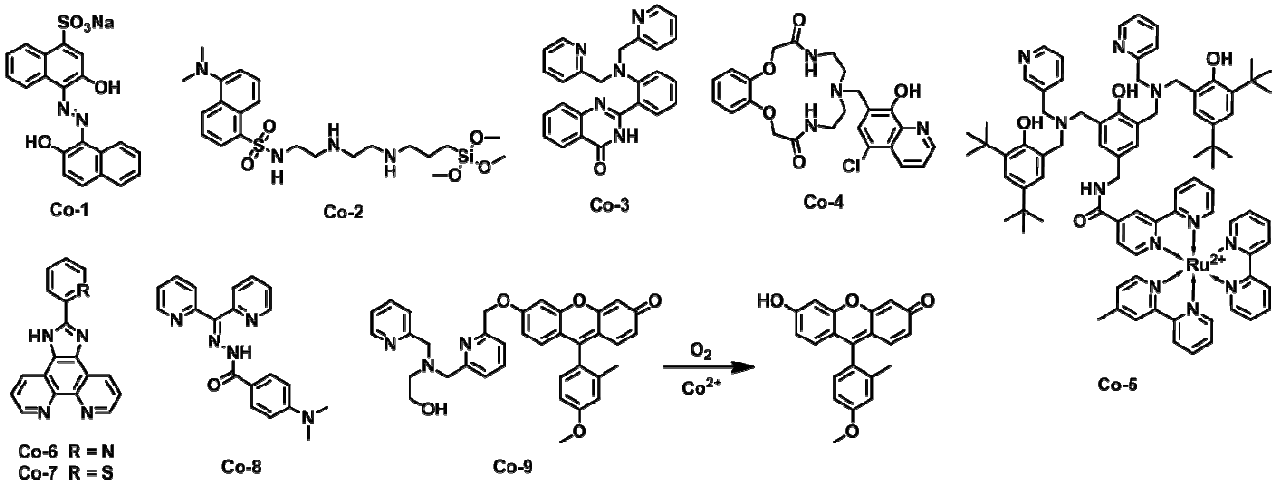

Montalti *et al*[198] have developed a fluorescent nanosensor for heavy metal ion by incorporating small-molecule sensors (**Co-2**) into silica colloids. These moieties possess a dansyl unit as a fluorophore and a polyamine chain as a receptor. The addition of Cu^{2+}, Co^{2+} or Ni^{2+} induces a strong quenching of the fluorescence intensity even at nanomolar concentrations. The high sensitivity is possible because the nanoparticle structure, in which a high density of sensor units is present, allows the occurrence of multicomponent cooperative photophysical processes. Sensor **Co-3** was synthesized by Zhang and co-workers[199] for sensing Co^{2+} using DPA as a recognition group and quinazoline as a reporting group. The fluorescence intensities of **Co-3** at 467 nm decrease with increasing concentration of Co^{2+}, which is attributed to cation-induced inhibition of ESIPT. Shamsipur *et al*[200] developed a cobalt sensing system by incorporating **Co-4** as a neutral cobalt-selective fluoroionophore in the plasticized PVC membrane containing sodium tetraphenylborate as a lipophilic anionic additive. The response of the sensor is based on the fluorescence quenching of **Co-4** by Co^{2+}. The optode membrane revealed good selectivity, reproducibility and high stability. An amide-

linked complex **Co-5**[201] designed by Zhang and co-workers, was used to recognize Co^{2+} in $C_2H_5OH–H_2O$ (1:1, v/v) solution, with the ruthenium(II) tris(bipyridine) moiety selected as a fluorophore and the multi-substituted phenol unit chosen as a receptor. Addition of Co^{2+} to **Co-5** resulted in a remarkable quenching of fluorescence signal. Other transition metal ions showed no obvious interference for Co^{2+} detection except Cu^{2+}. Wang *et al*[202] presented an ICT-based chromophore **Co-6** used as a sensor with a "turn-off" sensing capability for Co^{2+}. With the addition of Co^{2+} to **Co-6** in DMF under buffered conditions, a remarkable quenching of fluorescence signal was observed. Soon after, another phenanthroline-based compound (**Co-7**)[203] was designed by replacing pyridine with thiophene. **Co-7** could be used to detect K^+ ratiometricly and Co^{2+} with the phenomenon of fluorescence quenching.

"Turn-on" fluorescent sensors for Cobalt

Some fluorimetric methods[204-209] for the determination of cobalt were based on its fluorescence reactions with fluorophores and oxidizing agents such as hydrogen peroxide[205-209] and bromate[204]. These oxidization reactions can be divided into two types: one is the cobalt-catalytic oxidation of reduced fluorescein[206] or spiro form fluorescein-hydrazide[207] with hydrogen peroxide; the other is the oxidation of a ligand (PAPH[204], p-hydroxy-2-anilinopyridine[205], APTSQ[208], CPBSQ and FCPBSQ[209]) to a fluorescent product as the complex formation with cobalt ions. These proposed methods can output "turn-on" fluorescence signals and show high sensitivity (the detection limit was at nM/ng mL^{-1} level); however, oxidizing agents and the basic medium are required.

Besides, sensor **Co-8** along the lines of ICT concept, reported by Mashraqui and co-workers[210], exhibited Co^{2+} selective optical responses, which include 112 nm red shift in absorption (from 368 to 480 nm) and a dramatic 37-fold emission enhancement at 428 nm in the buffered $CH_3OH–H_2O$ (1:1 v/v) system. Further, Chang *et al*[211] developed a reaction-based sensor **Co-9** for selective "turn-on" fluorescence detection of Co^{2+}. **Co-9** displays weak fluorescence in 50 mM Tris buffer at pH 7.4, but treatment with Co^{2+} triggers a *ca*. 18-fold fluorescence increase within 2h resulting from cobalt-mediated oxidative C–O bond cleavage. The highly specific response of **Co-9** for Co^{2+} results from the dual requirement for metal binding and O_2 reactivity. Confocal experiments established that **Co-9** can reliably monitor increases or decreases in exchangeable Co^{2+} pools in living cells.

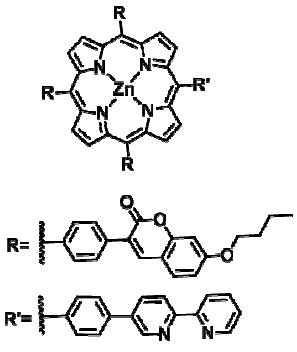

Co-10

Ratiometric fluorescent sensors for Cobalt

The only example of ratiometric fluorescent cobalt sensors, coumarin-zinc porphyrin-bipyridine **Co-10**[212], was developed by Lin and co-workers. The addition of cobalt induces a marked decrease (overall 7.5 fold) in the zinc porphyrin acceptor emission intensity around 606 nm and tremendous increase (overall 85.2 fold) in the coumarin donor fluorescence intensity around 432 nm. The EET efficiency of the sensor is modulated by the energy acceptor molar absorptivity variations upon cobalt binding, which is then transformed into a large ratiometric fluorescence response at two wavelengths. However, as paramagnetic Co^{2+} has fluorescence quenching nature, Co^{2+} needs to be oxidated to diamagnetic Co^{3+} by H_2O_2 in the assay experiment.

5.2 Colorimetric sensors for Cobalt

Kumar and co-workers[213] reported a differential chromogenic sensor **Co-11** for multi-ion (Co^{2+} and Ni^{2+}/Cu^{2+}) analysis. A solution of **Co-11** in sodium acetate-acetic acid buffer (pH 4.0) on addition of Co^{2+}, Ni^{2+} and Cu^{2+} gave respective blue (λ_{max} 620 nm), yellowish pink (λ_{max} 380, 460 and 510 nm) and yellow (λ_{max} 460 nm) colors. Govindaraju *et al*[12] developed a selective colorimetric sensor (**Co-12**) for Co^{2+} based on coumarin-conjugated thiocarbanohydrazone. Upon the addition of Co^{2+}, the absorbance band of **Co-12** at 470 nm red-shifted to 510 nm and the color of the solution changed from yellow to deep pink ascribed to the formation of a push-pull Co^{2+} Schiff base complex $[(\textbf{Co-12})_2Co]^{2+}$. *E. coli* exposed to Co^{2+} followed by **Co-12** developed a deep-pink color, indicating that the sensor could be used as a staining agent for Co^{2+} in microorganisms. A spiropyran-amide-DPA linkage (**Co-13**), developed by Shiraishi *et al*[214], showed selective colorimetric response to Co^{2+}. **Co-13** exists as a colorless spirocyclic (SP) form in the dark or under UV irradiation. UV irradiation of **Co-13** with Co^{2+}, however, leads to coloration with a strong merocyanine (MC) band at 472 nm. This is promoted by strong coordination of Co^{2+} with amide oxygen, leading to efficient photoisomerization of the spiropyran moieties. The isomerisation occurs at pH 7.0–12.0 and terminates within 1h. Other metal ions did not promote coloration and affect Co^{2+}-promote isomerisation except that addition of Cu^{2+} leads to significant decrease in the MC band.

A metal ion receptor **Co-14**, reported by Kim *et al*[215] and containing quinoline and pyridylaminophenol, acts as a colorimetric sensor for Co^{2+} by changing color from colorless to yellow. The color change is selective for Co^{2+} and found to be due to an absorption band that grows in at 465 nm. In a similar approach, the same group[216] developed a Co^{2+}-selective colorimetric sensor **Co-15** in a bis-tris buffer (10 mM, pH 7.0) solution containing 0.1% CH_3OH by the combination of julolidine and quinoline. Among the various metal ions, only Co^{2+} caused a distinct color change from yellow to orange. In the corresponding spectra, the absorption bands at 441 and 459 nm decreased and two new bands at 390 and 500 nm appeared.

Huang *et al*[217] developed leaf-like poly (*p*-phenylenediamine) (**Co-16**) microcrystal applied to the visual detection of Co^{2+}. **Co-16** could specifically interact with Co^{2+}, which results in a new strong absorption peak at 454 nm following the disappearance of the two absorption peaks at 342 and 540 nm. A noticeable purple-to-brown color change occurred within five minutes if Co^{2+} solution was mixed with **Co-16**, and Co^{2+} in the range 0.5–100 μM could be spectrometrically detected with the limit of

detection of 0.35 μM. The interaction between **Co-16** and Co^{2+} is identified to be an etching process. Etch cracks appear on the smooth surface of **Co-16** with the addition of Co^{2+} seen from the SEM images. Finally, a practical application of **Co-16** for light scattering imaging of Co^{2+} in fish tissues was developed.

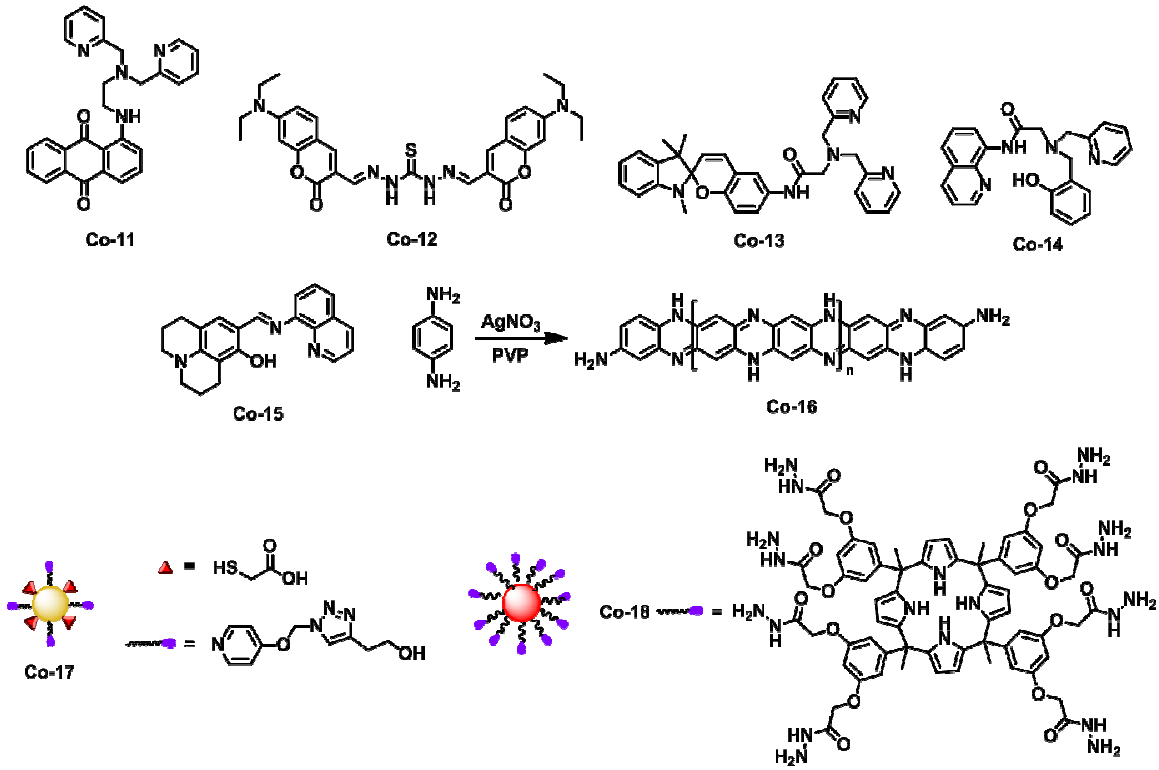

Li *et al*[218] developed bifunctionalized (triazole-carboxyl) AgNPs (**Co-17**) that have a cooperative effect on recognition of Co^{2+} over other metal ions tested. The presence of Co^{2+} ion induces a distinct color change from yellow to red. In the corresponding UV-vis spectra, Co^{2+} led to a decrease in absorption intensity at 405 nm, and a dramatic increase at 550 nm. **Co-17** became aggregated in solution in the presence of Co^{2+} through cooperative metal-ligand interaction. Jain and co-workers[219] developed water dispersible stable AuNPs as colorimetric sensors (**Co-18**) for selective signalling of Co^{2+}, in which calix[4]pyrrole octa-hydrazide (CPOH) acts as a reducing and stabilizing agent. Among all the metal ions investigated, only Co^{2+} ions gave sharp color change from ruby red to blue. The color change with Co^{2+} ions could be easily noticed even at nanomolar concentration. In the corresponding UV-vis spectrum, a 55 nm red shift was observed in the presence of Co^{2+}. In addition, **Co-18** showed fluorescence quenching at 698 nm towards Co^{2+}.

6. Nickel

Nickel plays important roles in the biology of microorganisms and plants[220] where it participates in a variety of cellular processes, particularly in energy and nitrogen metabolism[221]. Of the eight known nickel-containing enzymes, all but glyoxylase I catalyze the use and/or production of gases central to the global carbon, nitrogen, and oxygen cycles[221]. The average intake of nickel by humans ranges from 300–600 μg day^{-1}.[222-223] Loss of nickel homeostasis is harmful to both prokaryotic and eukaryotic organisms[224]. Nickel toxicity can result in adverse health effects ranging from allergic dermatitis to lung and nasal sinus cancers[225].

6.1 Fluorescent sensors for Nickel

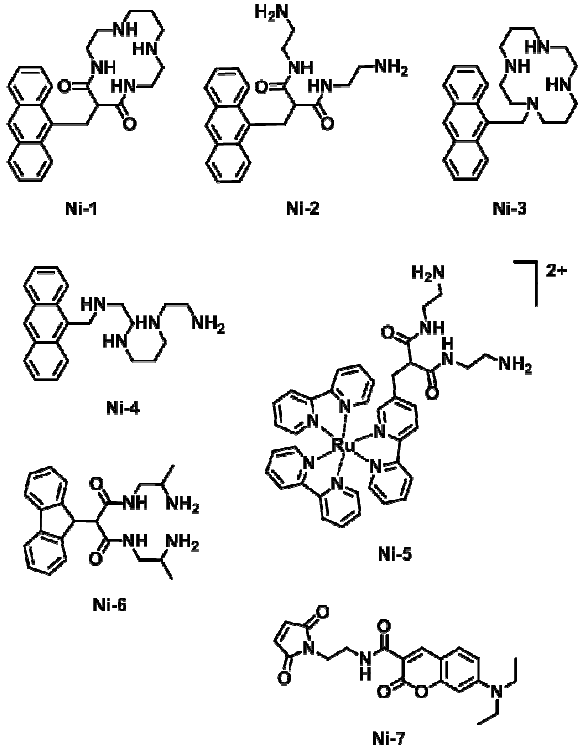

"Turn-off" fluorescent sensors for Nickel

A series of fluorescent sensors for Cu^{2+} and Ni^{2+} were designed by Fabbrizzi *et al*[226-227] using a supramolecular approach: an anthracene fragment (the signalling subunit) has been linked to either a cyclic (**Ni-1** and **Ni-3**) or a noncyclic (**Ni-2** and **Ni-4**) quadridentate ligand (the receptor). Occurrence of the metal-receptor interaction is signalled through the quenching of anthracene fluorescence based on a PET (**Ni-1** and **Ni-2**) or an energy-transfer (**Ni-3** and **Ni-4**) mechanism. However, one major drawback of these sensors is the need for organic/aqueous solvent mixtures as the working media due to the pronounced lipophilicity of the anthracene fragment. To improve this system's analytical practicability, the noncyclic dioxotetramine ligand of **Ni-2** was appended to the water-soluble $[Ru^{II}(bipy)_3]^{2+}$ unit (bipy = 2, 2'-bipyridine) to generate an efficient "turn-off" fluorescent sensor **Ni-5**[228] for sensing Ni^{2+} and Cu^{2+} in water. In addition, Luo *et al*[229] reported a ligand (**Ni-6**) consisting of fluorenyl and dioxotetraaza units. **Ni-6** can form a stable complex with Ni^{2+} accompanied by fluorescence quenching of the ligand, which is ascribed to electron transfer from the Ni^{2+} center to fluorenyl.

Daunert and co-workers[230] developed a sensing system (**NBP-Ni-7**) for Ni^{2+} based on the nickel binding protein (NBP) from *Escherichia coli* labelled with the fluorophore (**Ni-7**). When the NBP binds nickel, it undergoes a conformational change that can be used as the basis for an optical sensing system for nickel. In a spectrofluorimetric assay, there was a maximum of 65% quenching of the fluorescence signal produced by **NBP-Ni-7** in the presence of Ni^{2+}. Selectivity studies conducted with other divalent metals showed that fluorescence quenching for Co^{2+} was similar in magnitude but with much lower sensitivity than for Ni^{2+}. **NBP-Ni-7** was also used to develop assays in microtiter plate and fiber optic bundle formats.

"Turn-on" fluorescent sensors for Nickel

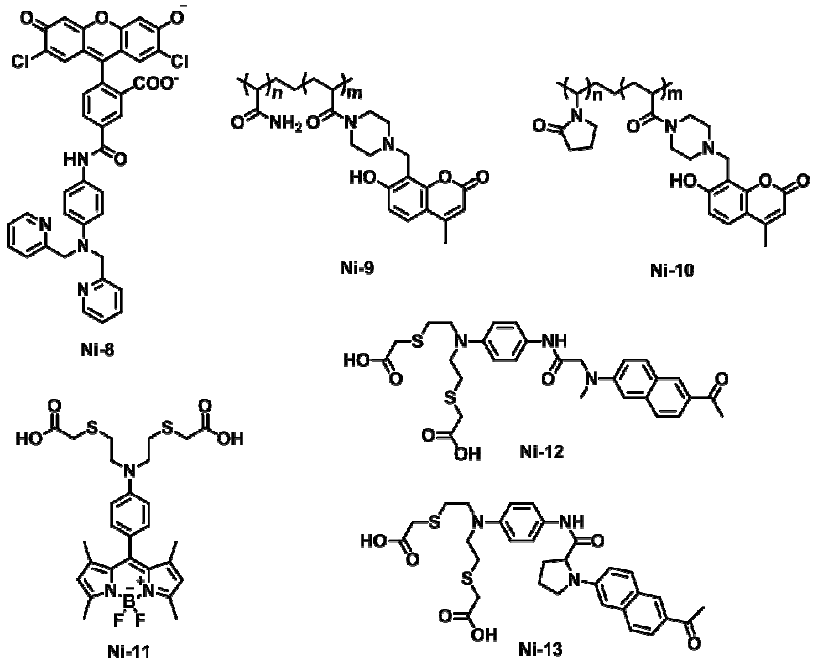

Newport Green DCF (**Ni-8**), a commercial metal-specific fluorescent indicator, has been demonstrated an exceptionally sensitive probe for Ni^{2+} in solution[231]. 100 μM Ni^{2+} enhances the fluorescence of **Ni-8** approximately 13-fold without a spectral shift[79]. The binding of metal ions at the DPA receptor unit will block the PET between DPA and the fluorophore and thus restore the fluorescence. **Ni-8** have been used to detect intracellular Ni^{2+} accumulation[232], measure the cellular uptake of Ni^{2+} in human monocyte-derived dendritic cells[233] and quantify Ni^{2+}-binding metalloproteins involved in human nickel allergy which is the most common form of human contact hypersensitivity[234].

Su and co-workers[235-236] synthesized an acrylic monomer bearing coumarin moieties, 7-hydroxy-4-methyl-8-(4'-acryloylpiperazin-1'-yl)methylcoumarin (Ac-HMPC). It was then copolymerized with acrylamide (AM)[235] or N-vinylpyrrolidone (VP)[236] to obtain water-soluble blue fluorescent materials, poly(Ac-HMPC-co-AM) (**Ni-9**) and poly(Ac-HMPC-co-VP) (**Ni-10**), respectively. The polymer sensors are selective to Ni^{2+}, with the increase in the fluorescence intensity depending on Ni^{2+} concentrations. The fluorescence enhancement was due to the piperazine ring acting as a ligand for Ni^{2+} and as a PET switch.

Chang and co-workers[237] have developed a "turn-on" fluorescent sensor **Ni-11** for the detection of Ni^{2+}. **Ni-11** combines a BODIPY dye reporter with *N*, *N*-bis[2-(carboxylmethyl) thioethyl]amine (CTEA) receptor to satisfy Ni^{2+}. It was proposed that the lone pair on the tertiary amine of CTEA was engaged in PET with the excited BODIPY fluorophore, which was responsible for the weak fluorescence of **Ni-11** (Φ = 0.002). Addition of 50 equiv of Ni^{2+} triggers a ca. 25-fold fluorescence enhancement (Φ = 0.055) with no emission maxima (λ_{em} = 507 nm) in 20 mM HEPES at pH 7.1. **Ni-11** did not yield a response in the presence of other biologically relevant metal ions. Confocal microscopy experiments show that this indicator can reliably monitor changes in Ni^{2+} levels within living mammalian cells. Cho *et al*[238] also chose CTEA as Ni^{2+} receptor and reported two fluorescent sensors (**Ni-12** and **Ni-13**). When Ni^{2+} was added to **Ni-12** or **Ni-13** in HEPES buffer, the fluorescence intensity increased gradually without affecting the

absorption spectrum, presumably because of the blocking of PET by the complexation with the metal ion. **Ni-13** gave much larger fluorescence enhancement factors (26) to Ni^{2+} for the one- and two-photon processes than **Ni-12** (5), which can be attributed to the introduction of the prolinamide ring reducing the vibrational relaxation pathways compared to the open-chain analogue (**Ni-12**). Both **Ni-12** and **Ni-13** showed high selectivity for Ni^{2+} over other metals. Finally, **Ni-13** was used to detect Ni^{2+} ions in fresh fish organs at 90–175 μm depth through TPM.

Table 1 Fluorescent peptidyl sensors

Peptide	Sequence[a]
Ni-14	Dap(**LR**[b])GlyHisDap(**DE**[c])SerSer-NH_2
Ni-15	Dap(**DE**)GlyHisDap(**LR**)SerSer-NH_2
Ni-16	Dap(**LR**)GlyHisDapSer(**DE**)Ser-NH_2
Ni-17	Dap(**LR**)GlyHisSerSerDap(**DE**)-NH_2
Ni-18	Dap(**LR**)AspHisDap(**DE**)SerSer-NH_2

a Fluorophores attached to the β-amine of the Dap residue are listed in brackets.

b **LR:** 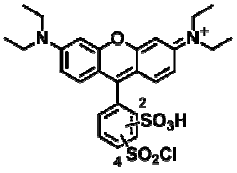

c **DE:** 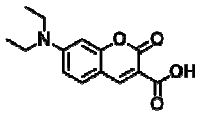

In addition, hexapeptides (**Ni-14**~**Ni-18**) incorporating two fluorophores (7-diethylaminocoumarin-3-carboxylic acid, DE, and lissamine rhodamine B sulfonyl chloride, LR) flanking a tripeptide sequence that binds Ni^{2+} and Cu^{2+} with high affinity were reported by Imperiali *et al*[239]. The fluorescence response of the peptides to each species is distinctly different: binding of Cu^{2+} by the sensor generates fluorescence quenching of both fluorophores, whereas binding of Ni^{2+} by the same species produces a FRET signal (the peak due to emission at 588 nm increased significantly).

6.2 Colorimetric sensors for Nickel

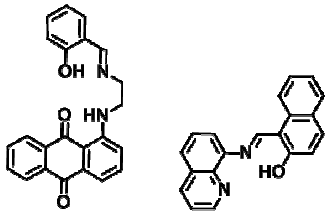

Ni-19 **Ni-20**

Kumar and co-workers[240] developed a colorimetric sensor (**Ni-19**) for simultaneous estimation of Cu^{2+} and Ni^{2+}. The absorbance properties of **Ni-19** were carried in 10 mM HEPES buffered CH_3OH–H_2O (4:1, v/v, pH 7.0 ± 0.1). On addition of Cu^{2+}, **Ni-19** shows ~100 nm red shift from λ_{max} 500 nm to 600 nm which induces a color change from red to blue. In the case of Ni^{2+}, a red shift ~250 nm from λ_{max} 500 nm to 750 nm with concomitant appearance of a new band at 385 nm is observed, which caused the color change from red to green. Zhang *et al*[241] described a quinoline derivative (**Ni-20**) which was used for the selective colorimetric detection of Ni^{2+}. A dramatic color change from yellow to red was observed by the naked eye upon the addition of Ni^{2+} to **Ni-20** in DMSO–HEPES buffer (1:1, v/v, pH 7.4). In the corresponding UV-vis spectra, the formation of a new absorption band at 525 nm and the decrease at 464 nm are consistant with this color change.

7. Conclusions

This critical review covers the chemical sensors for the first-row d-block metals (except Cu and Zn): Cr, Mn, Fe, Co, and Ni. Attention is given to the contributions of fluorescent sensors which are classified into three types: "turn-off", "turn-on", and ratiometric, colorimetric sensors, and responsive MRI contrast agents. Fluorescence imaging is a highly selective and sensitive technique with fast response times; colorimetry allows on-site and real-time detection and can be carried out by naked eyes; MRI offers the ability to capture three-dimensional images of living specimens with exquisite anatomical resolution. The successful development of systems that can detect the first-row transition metals based on these methods is clearly demonstrated. Duan *et al*[54] presented a simple FRET-based approach to ratiometric fluorescence sensing of Cr^{3+} in aqueous solution using glutathione and glucose as building blocks, inspired by the binding motifs of Cr^{3+} in GTF. Canary and co-workers[84] rationally designed a Mn^{2+}-selective ligand from bapta, which was further linked to a fluorescein fluorophore for the fluorescent sensing of Mn^{2+}. On the basis of hydroxylamine oxidization by Fe^{3+}, Chen *et al*[155] developed a BODIPY-based sensor for the selective detection of Fe^{3+}. Nagasawa *et al*[96] presented a Golgi-targeted fluorescent sensor for Fe^{2+} based on *N*-oxide chemistry. The only example of ratiometric fluorescent cobalt sensors, coumarin-zinc porphyrin-bipyridine, was reported by Lin and co-workers[212]. Huang *et al*[217] applied leaf-like poly (*p*-phenylenediamine) microcrystal to the visual detection of Co^{2+} in fish tissues based on an etching process. Chang *et al*[237] developed a Ni^{2+}-selective "turn-on" fluorescent sensor which combined a BODIPY dye with a CTEA receptor and was applied to imaging in living cells. Further, Cho group[238] linked the CTEA receptor to acedan, a two-photon fluorophore, for the detection of Ni^{2+} in fish organs. Merbach *et al*[127] developed a bipyridine-based heterotritopic ligand which could self-assemble with Fe^{2+} and Gd^{3+} into a metallostar structure, with a much larger relaxivity compared with its parent Gd^{3+} complex.

However, there is still much scope to improve theses sensors: 1) sensors for Sc, Ti, and V need further investigation; 2) responsive MRI contrast agents for Cr, Mn, Co, Ni are still blank; 3) further development of ratiometric fluorescent sensors for Cr^{6+}, Mn^{2+}, and Ni^{2+} is necessary; 4) many of the sensors for Cr^{3+} and Fe^{3+} only work in pure organic or unbuffered aqueous solutions, while Cr^{3+} and Fe^{3+} are known to hydrolyze in water releasing protons which may interfere the metal sensing; 5) it is still a challenge to apply MRI sensors in living systems. In addition, given that fluorescence imaging is difficult at more than a few millimetres in depth within a tissue specimen and MRI has low selectivity and sensitivity, dual-modality (combined MRI/fluorescence) imaging can provide more information on

targeted molecules than a single imaging modality and is useful for biomedical research and clinical practice[242]. On the basis of the advantages of the fluorometric, MRI, and colorimetric methods and these existing challenges, we hope further investigation and development of sensors for the first-row d-block metal ions.

Acknowledgements

This work was financially supported by NSF of China (21136002, 21422601 and 21421005), National Basic Research Program of China (2013CB733702), Ministry of Education (NCET-12-0080), Liaoning NSF (2013020115) and Fundamental Research Funds for the Central University (DUT14ZD214).

Notes and references

[a] *State Key Laboratory of Fine Chemicals, Dalian University of Technology, No. 2 Linggong Road, High-tech District, Dalian 116024, China. Fax: +86 411 84986306; Tel:+86 411 84986327; E-mail: fanjl@dlut.edu.cn, pengxj@dlut.edu.cn*

1 K. P. Carter, A. M. Young and A. E. Palmer, *Chem. Rev.*, 2014, 114, 4564-4601.
2 T. McKee and J. R. McKee, *Biochemistry: An Introduction*, McGraw-Hill Companies, Inc. New York, China Science Press, 2nd edn, 1999.
3 C. K. Mathews and K. E. Van Holde, *Biochemistry*, The Benjamin/Cummings Publishing Company, Inc. Menlo Park, 2nd edn, 1996.
4 C. S. Bonnet and É. Tóth, *Future Med. Chem.*, 2010, 2, 367-384.
5 T. W. Bell and N. M. Hext, *Chem. Soc. Rev.*, 2004, 33, 589-598.
6 J. Mao, L. Wang, W. Dou, X. Tang, Y. Yan and W. Liu, *Org. Lett.*, 2007, 9, 4567-4570.
7 X. Lu, W. Zhu, Y. Xie, X. Li, Y. Gao, F. Li and H. Tian, *Chem. Eur. J.*, 2010, 16, 8355-8364.
8 R. Y. Tsien, *Fluorescent and Photochemical Probes of Dynamic Biochemical Signals inside Living Cells*, ed. A. W. Czarnik, American Chemical Society, Washington DC, 1993.
9 M. Formica, V. Fusi, L. Giorgi and M. Micheloni, *Coord. Chem. Rev.*, 2012, 256, 170-192.
10 S. K. Sahoo, D. Sharma, R. K. Bera, G. Crisponi and J. F. Callan, *Chem. Soc. Rev.*, 2012, 41, 7195-7227.
11 D. Xiong and H. Li, *Nanotechnology*, 2008, 19, 465502-465508.
12 D. Maity and T. Govindaraju, *Inorg. Chem.*, 2011, 50, 11282-11284.
13 E. L. Que and C. J. Chang, *Chem. Soc. Rev.*, 2010, 39, 51-60.
14 J. Costa, R. Ruloff, L. Burai, L. Helm and A. E. Merbach, *J. Am. Chem. Soc.*, 2005, 127, 5147-5157.
15 M. C. Heffern, L. M. Matosziuk and T. J. Meade, *Chem. Rev.*, 2013, 114, 4496-4539.
16 A. Zayed and N. Terry, *Plant Soil*, 2003, 249, 139-156.
17 W. T. Cefalu and F. B. Hu, *Diabetes Care*, 2004, 27, 2741-2751.
18 A. K. Singh, V. K. Gupta and B. Gupta, *Anal. Chim. Acta*, 2007, 585, 171-178.
19 J. B. Vincent, *Nutr. Rev.*, 2000, 58, 67-72.
20 M. Zhang, Z. Chen, Q. Chen, H. Zou, J. Lou and J. He, *Mutat. Res-Genet. Toxicol. E. M.*, 2008, 654, 45-51.
21 M. Costa and C. B. Klein, *CRC Crit. Rev. Toxicol.*, 2006, 36, 155-163.
22 F. Y. Saleh, G. E. Mbamalu, Q. H. Jaradat and C. E. Brungardt, *Anal. Chem.*, 1996, 68, 740-745.
23 L. Zhang, J. Wang, J. Fan, K. Guo and X. Peng, *Bioorg. Med. Chem. Lett.*, 2011, 21, 5413-5416.
24 B. Tang, T. Yue, J. Wu, Y. Dong, Y. Ding and H. Wang, *Talanta*, 2004, 64, 955-960.
25 D. Karak, A. Banerjee, A. Sahana, S. Guha, S. Lohar, S. S. Adhikari and D. Das, *J. Hazard. Mater.*, 2011, 188, 274-280.
26 A. P. de Silva, T. Gunnlaugsson and T. E. Rice, *Analyst*, 1996, 121, 1759-1762.
27 R. A. Bissell, A. P. de Silva, H. Q. N. Gunaratne, P. L. M. Lynch, G. E. M. Maguire and K. R. A. S. Sandanayake, *Chem. Soc. Rev.*, 1992, 21, 187-195.
28 J. F. Callan, A. P. de Silva and D. C. Magri, *Tetrahedron*, 2005, 61, 8551-8588.
29 M. Sarkar, S. Banthia and A. Samanta, *Tetrahedron Lett.*, 2006, 47, 7575-7578.
30 D. Wang, Y. Shiraishi and T. Hirai, *Tetrahedron Lett.*, 2010, 51, 2545-2549.
31 Z. Li, W. Zhao, Y. Zhang, L. Zhang, M. Yu, J. Liu and H. Zhang, *Tetrahedron*, 2011, 67, 7096-7100.
32 S. Wu, K. Zhang, Y. Wang, D. Mao, X. Liu, J. Yu and L. Wang, *Tetrahedron Lett.*, 2014, 55, 351-353.
33 S. Guha, S. Lohar, A. Banerjee, A. Sahana, I. Hauli, S. K. Mukherjee, J. S. Matalobos and D. Das, *Talanta*, 2012, 91, 18-25.
34 H. Kim, K. B. Kim, E. J. Song, I. H. Hwang, J. Y. Noh, P.-G. Kim, K.-D. Jeong and C. Kim, *Inorg. Chem. Commun.*, 2013, 36, 72-76.
35 X. Chen, T. Pradhan, F. Wang, J. S. Kim and J. Yoon, *Chem. Rev.*, 2011, 112, 1910-1956.
36 H. N. Kim, M. H. Lee, H. J. Kim, J. S. Kim and J. Yoon, *Chem. Soc. Rev.*, 2008, 37, 1465-1472.
37 K. Huang, H. Yang, Z. Zhou, M. Yu, F. Li, X. Gao, T. Yi and C. Huang, *Org. Lett.*, 2008, 10, 2557-2560.
38 J. Mao, Q. He and W. Liu, *Anal Bioanal Chem*, 2010, 396, 1197-1203.
39 Q. Meng, W. Su, X. Hang, X. Li, C. He and C. Duan, *Talanta*, 2011, 86, 408-414.
40 A. J. Weerasinghe, C. Schmiesing and E. Sinn, *Tetrahedron Lett.*, 2009, 50, 6407-6410.
41 Y. Zhou, J. Zhang, L. Zhang, Q. Zhang, T. Ma and J. Niu, *Dyes Pigm.*, 2013, 97, 148-154.
42 S. Saha, P. Mahato, U. R. G, E. Suresh, A. Chakrabarty, M. Baidya, S. K. Ghosh and A. Das, *Inorg. Chem.*, 2011, 51, 336-345.
43 D. Liu, T. Pang, K. Ma, W. Jiang and X. Bao, *RSC Adv.*, 2014, 4, 2563-2567.
44 P. Mahato, S. Saha, E. Suresh, R. Di Liddo, P. P. Parnigotto, M. T. Conconi, M. K. Kesharwani, B. Ganguly and A. Das, *Inorg. Chem.*, 2012, 51, 1769-1777.
45 H. Wu, P. Zhou, J. Wang, L. Zhao and C. Duan, *New J. Chem.*, 2009, 33, 653-658.
46 J. Y. Jung, S. J. Han, J. Chun, C. Lee and J. Yoon, *Dyes Pigm.*, 2012, 94, 423-426.

47 V. Bravo, S. Gil, A. M. Costero, M. N. Kneeteman, U. Llaosa, P. M. E. Mancini, L. E. Ochando and M. Parra, *Tetrahedron*, 2012, 68, 4882-4887.

48 S. Goswami, A. K. Das, A. K. Maity, A. Manna, K. Aich, S. Maity, P. Saha and T. K. Mandal, *Dalton Trans.*, 2014, 43, 231-239.

49 M. Mukherjee, B. Sen, S. Pal, M. S. Hundal, S. K. Mandal, A. R. Khuda-Bukhsh and P. Chattopadhyay, *RSC Adv.*, 2013, 3, 19978-19984.

50 J. Fan, M. Hu, P. Zhan and X. Peng, *Chem. Soc. Rev.*, 2013, 42, 29-43.

51 R. Y. Tsien and A. T. Harootunian, *Cell Calcium*, 1990, 11, 93-109.

52 Z. Zhou, M. Yu, H. Yang, K. Huang, F. Li, T. Yi and C. Huang, *Chem. Commun.*, 2008, 3387-3389.

53 Y. Wan, Q. Guo, X. Wang and A. Xia, *Anal. Chim. Acta*, 2010, 665, 215-220.

54 X. Hu, X. Zhang, G. He, C. He and C. Duan, *Tetrahedron*, 2011, 67, 1091-1095.

55 P. Saluja, H. Sharma, N. Kaur, N. Singh and D. O. Jang, *Tetrahedron*, 2012, 68, 2289-2293.

56 Y. J. Jang, Y. H. Yeon, H. Y. Yang, J. Y. Noh, I. H. Hwang and C. Kim, *Inorg. Chem. Commun.*, 2013, 33, 48-51.

57 L. Jiang, Y. Sun, F. Huo, H. Zhang, L. Qin, S. Li and X. Chen, *Nanoscale*, 2012, 4, 66-75.

58 R. Klajn, J. F. Stoddart and B. A. Grzybowski, *Chem. Soc. Rev.*, 2010, 39, 2203-2237.

59 J. Du, Q. Shao, S. Yin, L. Jiang, J. Ma and X. Chen, *Small*, 2012, 8, 3412-3416.

60 K. Saha, S. S. Agasti, C. Kim, X. Li and V. M. Rotello, *Chem. Rev.*, 2012, 112, 2739-2779.

61 Y.-W. Lin, C.-C. Huang and H.-T. Chang, *Analyst*, 2011, 136, 863-871.

62 H. Jans and Q. Huo, *Chem. Soc. Rev.*, 2012, 41, 2849-2866.

63 D. Liu, Z. Wang and X. Jiang, *Nanoscale*, 2011, 3, 1421-1433.

64 L. Zhao, Y. Jin, Z. Yan, Y. Liu and H. Zhu, *Anal. Chim. Acta*, 2012, 731, 75-81.

65 Y.-C. Chen, I. L. Lee, Y.-M. Sung and S.-P. Wu, *Sens. Actuators, B*, 2013, 188, 354-359.

66 N. Jie, Q. Zhang, J. Yang and X. Huang, *Talanta*, 1998, 46, 215-219.

67 T. M. A. Razek, S. Spear, S. S. M. Hassan and M. A. Arnold, *Talanta*, 1999, 48, 269-275.

68 L. Wang, L. Wang, T. Xia, L. Dong, H. Chen and L. Li, *Spectrochim. Acta, Part A*, 2004, 60, 2465-2468.

69 L. Wang, L. Wang, T. Xia, L. Dong, G. Bian and H. Chen, *Anal. Sci.*, 2004, 20, 1013-1017.

70 S. J. Toal, K. A. Jones, D. Magde and W. C. Trogler, *J. Am. Chem. Soc.*, 2005, 127, 11661-11665.

71 M. Hosseini, V. K. Gupta, M. R. Ganjali, Z. Rafiei-Sarmazdeh, F. Faridbod, H. Goldooz, A. R. Badiei and P. Norouzi, *Anal. Chim. Acta*, 2012, 715, 80-85.

72 H. Chen and J. Ren, *Talanta*, 2012, 99, 404-408.

73 D. Zhang, Z. Dong, X. Jiang, M. Feng, W. Li and G. Gao, *Anal. Methods*, 2013, 5, 1669-1675.

74 Y. Xiang, L. Mei, N. Li and A. Tong, *Anal. Chim. Acta*, 2007, 581, 132-136.

75 J.-H. Ye, Y. Wang, Y. Bai, W. Zhang and W. He, *RSC Adv.*, 2014, 4, 2989-2992.

76 F. Tan, X. Liu, X. Quan, J. Chen, X. Li and H. Zhao, *Anal. Methods*, 2011, 3, 343-347.

77 A. Sigel and H. Sigel, *Metal Ions In Biological Systems*, Marcel Dekker Inc. New York, 2000.

78 N. A. Law, M. T. Caudle and V. L. Pecoraro, in *Advances in Inorganic Chemistry*, ed. A. G. Sykes, Academic Press, 1998.

79 F. Galiazzo, J. Pedersen, P. Civitareale, A. Schiesser and G. Rotilio, *Biol. Metals*, 1989, 2, 6-10.

80 S. Xu, C. Wang, H. Zhang, Q. Sun, Z. Wang and Y. Cui, *J. Mater. Chem.*, 2012, 22, 9216-9221.

81 J. A. Roth, *Biol. Res.*, 2006, 39, 45-57.

82 R. P. Haugland, *Handbook of Fluorescent Probes and Research Products*, Molecular Probes, chap. 19.

83 F. Gruppi, J. Liang, B. B. Bartelle, M. Royzen, D. H. Turnbull and J. W. Canary, *Chem. Commun.*, 2012, 48, 10778-10780.

84 J. Liang and J. W. Canary, *Angew. Chem. Int. Ed.*, 2010, 49, 7710-7713.

85 R. Y. Tsien, *Biochemistry*, 1980, 19, 2396-2404.

86 X. Mao, H. Su, D. Tian, H. Li and R. Yang, *ACS Appl. Mater. Interfaces*, 2013, 5, 592-597.

87 F. B. Serrat, *Microchim. Acta*, 1998, 129, 77-80.

88 K. L. Mutaftchiev, *Anal. Lett.*, 2004, 37, 2869-2879.

89 J. Maly and H. Fadrus, *Analyst*, 1974, 99, 128-136.

90 W. F. Beyer Jr and I. Fridovich, *Anal. Biochem.*, 1988, 170, 512-519.

91 Z. Dai, N. Khosla and J. W. Canary, *Supramol. Chem.*, 2009, 21, 296-300.

92 S. Epsztejn, H. Glickstein, V. Picard, I. N. Slotki, W. Breuer, C. Beaumont and Z. I. Cabantchik, *Blood*, 1999, 94, 3593-3603.

93 S. J. Lippard and J. M. Berg, *Principles of Bioinorganic Chemistry*, University Science Books, Mill Valley, CA, 1994.

94 A. Jacobs, *Blood*, 1977, 50, 433-439.

95 R. C. Hider and X. Kong, *Dalton Trans.*, 2013, 42, 3220-3229.

96 T. Hirayama, K. Okuda and H. Nagasawa, *Chem. Sci.*, 2013, 4, 1250-1256.

97 J. Xu, Z. Jia, M. D. Knutson and C. Leeuwenburgh, *Int. J. Mol. Sci.*, 2012, 13, 2368-2386.

98 S. Toyokuni, *Cancer Sci.*, 2009, 100, 9-16.

99 K. V. Kowdley, *Gastroenterology*, 2004, 127, S79-S86.

100 F. Molina-Holgado, R. Hider, A. Gaeta, R. Williams and P. Francis, *BioMetals*, 2007, 20, 639-654.

101 W. B. a. Z. I. C. B. P. Esposito, *Biochem. Soc. Trans.*, 2002, 30, 729-732.

102 B. P. Espósito, S. Epsztejn, W. Breuer and Z. I. Cabantchik, *Anal. Biochem.*, 2002, 304, 1-18.

103 W. Breuer, S. Epsztejn and Z. I. Cabantchik, *J. Biol. Chem.*, 1995, 270, 24209-24215.

104 W. Breuer, S. Epsztejn, P. Millgram and I. Z. Cabantchik, *Am. J. Physiol. Cell Physiol.*, 1995, 268, C1354-C1361.

105 W. Breuer, S. Epsztejn and Z. Ioav Cabantchik, *FEBS Lett.*, 1996, 382, 304-308.

106 S. Epsztejn, O. Kakhlon, H. Glickstein, W. Breuer and Z. I. Cabantchik, *Anal. Biochem.*, 1997, 248, 31-40.

107 A. Ali, Q. Zhang, J. Dai and X. Huang, *BioMetals*, 2003, 16, 285-293.

108 F. Petrat, U. Rauen and H. de Groot, *Hepatology*, 1999, 29, 1171-1179.

109 F. Petrat, H. de Groot and U. Rauen, *Arch. Biochem. Biophys.*, 2000, 376, 74-81.

110 F. Petrat, H. de Groot and U. Rauen, *Biochem. J.*, 2001, 356, 61-69.

111 F. Petrat, D. Weisheit, M. Lensen, H. de Groot, R. Sustmann and U. Rauen, *Biochem. J.*, 2002, 362, 137-147.

112 I. Grabchev, J.-M. Chovelon and V. Bojinov, *Polym. Adv. Technol.*, 2004, 15, 382-386.

113 P. Wu, Y. Li and X.-P. Yan, *Anal. Chem.*, 2009, 81, 6252-6257.

114 L.-J. Fan and W. E. Jones, *J. Am. Chem. Soc.*, 2006, 128, 6784-6785.

115 L. Praveen, M. L. P. Reddy and R. L. Varma, *Tetrahedron Lett.*, 2010, 51, 6626-6629.

116 J.-L. Chen, S.-J. Zhuo, Y.-Q. Wu, F. Fang, L. Li and C.-Q. Zhu, *Spectrochim. Acta, Part A*, 2006, 63, 438-443.

117 M. Niwa, T. Hirayama, K. Okuda and H. Nagasawa, *Org. Biomol. Chem.*, 2014, 12, 6590-6597.

118 H. Y. Au-Yeung, J. Chan, T. Chantarojsiri and C. J. Chang, *J. Am. Chem. Soc.*, 2013, 135, 15165-15173.

119 P. Li, L. Fang, H. Zhou, W. Zhang, X. Wang, N. Li, H. Zhong and B. Tang, *Chem. Eur. J.*, 2011, 17, 10520-10523.

120 K. B. Kim, H. Kim, E. J. Song, S. Kim, I. Noh and C. Kim, *Dalton Trans.*, 2013, 42, 16569-16577.

121 Y. W. Choi, G. J. Park, Y. J. Na, H. Y. Jo, S. A. Lee, G. R. You and C. Kim, *Sens. Actuators, B*, 2014, 194, 343-352.

122 H. Kim, Y. J. Na, E. J. Song, K. B. Kim, J. M. Bae and C. Kim, *RSC Adv.*, 2014, 4, 22463-22469.

123 R. Ruloff, G. v. Koten and A. E. Merbach, *Chem. Commun.*, 2004, 842-843.

124 W.-S. Li, J. Luo and Z.-N. Chen, *Inorg. Chem. Commun.*, 2011, 14, 1898-1900.

125 T. N. Parac-Vogt, L. Vander Elst, K. Kimpe, S. Laurent, C. Burtéa, F. Chen, R. Van Deun, Y. Ni, R. N. Muller and K. Binnemans, *Contrast Media Mol. Imaging*, 2006, 1, 267-278.

126 J. Paris, C. Gameiro, V. Humblet, P. K. Mohapatra, V. Jacques and J. F. Desreux, *Inorg. Chem.*, 2006, 45, 5092-5102.

127 J. B. Livramento, É. Tóth, A. Sour, A. Borel, A. E. Merbach and R. Ruloff, *Angew. Chem. Int. Ed.*, 2005, 44, 1480-1484.

128 J. B. Livramento, C. Weidensteiner, M. I. M. Prata, P. R. Allegrini, C. F. G. C. Geraldes, L. Helm, R. Kneuer, A. E. Merbach, A. C. Santos, P. Schmidt and É. Tóth, *Contrast Media Mol. Imaging*, 2006, 1, 30-39.

129 X. Qu, Q. Liu, X. Ji, H. Chen, Z. Zhou and Z. Shen, *Chem. Commun.*, 2012, 48, 4600-4602.

130 P.-E. Danjou, J. Lyskawa, F. Delattre, M. Becuwe, P. Woisel, S. Ruellan, S. Fourmentin and F. Cazier-Dennin, *Sens. Actuators, B*, 2012, 171–172, 1022-1028.

131 J. Liu, Y.-Q. Xie, Q. Lin, B.-B. Shi, P. Zhang, Y.-M. Zhang and T.-B. Wei, *Sens. Actuators, B*, 2013, 186, 657-665.

132 S. Hu, G. Wu, C. Xu, J. Dong and Q. Gao, *J. Photochem. Photobiol. A*, 2013, 270, 37-42.

133 M. Yang, M. Sun, Z. Zhang and S. Wang, *Talanta*, 2013, 105, 34-39.

134 D. En, Y. Guo, B.-T. Chen, B. Dong and M.-J. Peng, *RSC Adv.*, 2014, 4, 248-253.

135 F. Gai, X. Li, T. Zhou, X. Zhao, D. Lu, Y. Liu and Q. Huo, *J. Mater. Chem. B*, 2014, 2, 6306-6312.

136 J. S. Kim and D. T. Quang, *Chem. Rev.*, 2007, 107, 3780-3799.

137 M. Kumar, R. Kumar and V. Bhalla, *Tetrahedron Lett.*, 2010, 51, 5559-5562.

138 M. Kumar, R. Kumar and V. Bhalla, *Org. Lett.*, 2010, 13, 366-369.

139 M. Kumar, R. Kumar, V. Bhalla, P. R. Sharma, T. Kaur and Y. Qurishi, *Dalton Trans.*, 2012, 41, 408-412.

140 Z. Yang, M. She, B. Yin, J. Cui, Y. Zhang, W. Sun, J. Li and Z. Shi, *J. Org. Chem.*, 2011, 77, 1143-1147.

141 N. R. Chereddy, K. Suman, P. S. Korrapati, S. Thennarasu and A. B. Mandal, *Dyes Pigm.*, 2012, 95, 606-613.

142 N. R. Chereddy, S. Thennarasu and A. B. Mandal, *Dalton Trans.*, 2012, 41, 11753-11759.

143 L. Huang, F. Hou, J. Cheng, P. Xi, F. Chen, D. Bai and Z. Zeng, *Org. Biomol. Chem.*, 2012, 10, 9634-9638.

144 S.-R. Liu and S.-P. Wu, *Sens. Actuators, B*, 2012, 171–172, 1110-1116.

145 J. Bordini, I. Calandreli, G. O. Silva, K. Q. Ferreira, D. P. S. Leitão-Mazzi, E. M. Espreafico and E. Tfouni, *Inorg. Chem. Commun.*, 2013, 35, 255-259.

146 B. Rathinam, C.-C. Chien, B.-C. Chen and J.-H. Liu, *Tetrahedron*, 2013, 69, 235-241.

147 V. Bhalla, N. Sharma, N. Kumar and M. Kumar, *Sens. Actuators, B*, 2013, 178, 228-232.

148 C.-Y. Li, C.-X. Zou, Y.-F. Li, J.-L. Tang and C. Weng, *Dyes Pigm.*, 2014, 104, 110-115.

149 S. Goswami, S. Das, K. Aich, D. Sarkar, T. K. Mondal, C. K. Quah and H.-K. Fun, *Dalton Trans.*, 2013, 42, 15113-15119.

150 S. Ji, X. Meng, W. Ye, Y. Feng, H. Sheng, Y. Cai, J. Liu, X. Zhu and Q. Guo, *Dalton Trans.*, 2014, 43, 1583-1588.

151 J. Huang, Y. Xu and X. Qian, *Dalton Trans.*, 2014, 43, 5983-5989.

152 L. Wang, H. Li and D. Cao, *Sens. Actuators, B*, 2013, 181, 749-755.

153 L. Yang, W. Zhu, M. Fang, Q. Zhang and C. Li, *Spectrochim. Acta, Part A*, 2013, 109, 186-192.

154 Z. Li, Y. Zhou, K. Yin, Z. Yu, Y. Li and J. Ren, *Dyes Pigm.*, 2014, 105, 7-11.

155 R. Wang, F. Yu, P. Liu and L. Chen, *Chem. Commun.*, 2012, 48, 5310-5312.

156 L. Yang, W. Yang, D. Xu, Z. Zhang and A. Liu, *Dyes Pigm.*, 2013, 97, 168-174.

157 S. Sen, S. Sarkar, B. Chattopadhyay, A. Moirangthem, A. Basu, K. Dhara and P. Chattopadhyay, *Analyst*, 2012, 137, 3335-3342.

158 Z.-X. Li, W. Zhou, L.-F. Zhang, R.-L. Yuan, X.-J. Liu, L.-H. Wei and M.-M. Yu, *J. Lumin.*, 2013, 136, 141-144.

159 S.-d. Liu, L.-w. Zhang and X. Liu, *New J. Chem.*, 2013, 37, 821-826.

160 F. Ge, H. Ye, H. Zhang and B.-X. Zhao, *Dyes Pigm.*, 2013, 99, 661-665.

161 N. R. Chereddy, S. Thennarasu and A. B. Mandal, *Analyst*, 2013, 138, 1334-1337.

162 Y.-X. Wu, J.-B. Li, L.-H. Liang, D.-Q. Lu, J. Zhang, G.-J. Mao, L.-Y. Zhou, X.-B. Zhang, W. Tan, G.-L. Shen and R.-Q. Yu, *Chem. Commun.*, 2014, 50, 2040-2042.

163 K. J. Wallace, M. Gray, Z. Zhong, V. M. Lynch and E. V. Anslyn, *Dalton Trans.*, 2005, 2436-2441.

164 Z.-Q. Liang, C.-X. Wang, J.-X. Yang, H.-W. Gao, Y.-P. Tian, X.-T. Tao and M.-H. Jiang, *New J. Chem.*, 2007, 31, 906-910.

165 A. Mitra, B. Ramanujam and C. P. Rao, *Tetrahedron Lett.*, 2009, 50, 776-780.

166 D. Wei, Y. Sun, J. Yin, G. Wei and Y. Du, *Sens. Actuators, B*, 2011, 160, 1316-1321.

167 P. Suresh, I. A. Azath and K. Pitchumani, *Sens. Actuators, B*, 2010, 146, 273-277.

168 S. A. BK Adebayo, HK Okoro, BJ Ximba, *Afr. J. Biotechnol.*, 2011, 10, 16051-16057.

169 N. Narayanaswamy and T. Govindaraju, *Sens. Actuators, B*, 2012, 161, 304-310.

170 P. Kaur and D. Sareen, *Dyes Pigm.*, 2011, 88, 296-300.

171 S. Devaraj, Y.-k. Tsui, C.-Y. Chiang and Y.-P. Yen, *Spectrochim. Acta, Part A*, 2012, 96, 594-599.

172 R.-L. Liu, H.-Y. Lu, M. Li, S.-Z. Hu and C.-F. Chen, *RSC Adv.*, 2012, 2, 4415-4420.

173 T.-B. Wei, P. Zhang, B.-B. Shi, P. Chen, Q. Lin, J. Liu and Y.-M. Zhang, *Dyes Pigm.*, 2013, 97, 297-302.

174 L. Hu, L. Nie, G. Xu, H. Shi, X. Xu, X. Zhang and Z. Yan, *RSC Adv.*, 2014, 4, 19370-19374.

175 S.-P. Wu, Y.-P. Chen and Y.-M. Sung, *Analyst*, 2011, 136, 1887-1891.

176 V. N. Mehta, S. K. Kailasa and H.-F. Wu, *New J. Chem.*, 2014, 38, 1503-1511.

177 S. K. Tripathy, J. Y. Woo and C.-S. Han, *Sens. Actuators, B*, 2013, 181, 114-118.

178 J.-M. Liu, X.-X. Wang, L. Jiao, M.-L. Cui, L.-P. Lin, L.-H. Zhang and S.-L. Jiang, *Talanta*, 2013, 116, 199-204.

179 H. Wei, C. Chen, B. Han and E. Wang, *Anal. Chem.*, 2008, 80, 7051-7055.

180 J. Zhan, L. Wen, F. Miao, D. Tian, X. Zhu and H. Li, *New J. Chem.*, 2012, 36, 656-661.

181 A. Pandya, P. G. Sutariya, A. Lodha and S. K. Menon, *Nanoscale*, 2013, 5, 2364-2371.

182 S. Bothra, J. N. Solanki, S. K. Sahoo and J. F. Callan, *RSC Adv.*, 2014, 4, 1341-1346.

183 S. Aime, M. Botta, M. Fasano and E. Terreno, *Spectrochim. Acta, Part A*, 1993, 49, 1315-1322.

184 T. N. Parac-Vogt, K. Kimpe and K. Binnemans, *J. Alloys Compd.*, 2004, 374, 325-329.

185 V. Jacques and J. Desreux, in *Contrast Agents I*, ed. W. Krause, Springer Berlin Heidelberg, 2002.

186 V. C. Pierre, M. Botta, S. Aime and K. N. Raymond, *J. Am. Chem. Soc.*, 2006, 128, 9272-9273.

187 S. Okamoto and L. D. Eltis, *Metallomics*, 2011, 3, 963-970.

188 E. Raux, H. L. Schubert and M. J. Warren, *Cell. Mol. Life Sci.*, 2000, 57, 1880-1893.

189 M. Kobayashi and S. Shimizu, *Eur. J. Biochem.*, 1999, 261, 1-9.

190 Z. Y. Zhang, *Stud. Trace Elem. Health*, 1996, 21, 3.

191 B. Venugopal and T. D. Luckey, *Metal Toxicity In Mammals*, Plenum Press, New York, 1979.

192 I. Paris and J. J. B. Jones,*The Handbook of Trace Elements*, St. Lucie Press, Florida, 1997.

193 S. B. Zamochnick and G. A. Rechnitz, *Z. Anal. Chem.*, 1964, 199, 424-429.

194 F. Monteil-Rivera and J. Dumonceau, *Anal Bioanal Chem*, 2002, 374, 1105-1112.

195 R. A. Saar and J. H. Weber, *Anal. Chem.*, 1980, 52, 2095-2100.

196 D. K. Ryan and J. H. Weber, *Anal. Chem.*, 1982, 54, 986-990.

197 J. C. Westall, J. D. Jones, G. D. Turner and J. M. Zachara, *Environ. Sci. Technol.*, 1995, 29, 951-959.

198 M. Montalti, L. Prodi and N. Zaccheroni, *J. Mater. Chem.*, 2005, 15, 2810-2814.

199 H.-Y. Luo, X.-B. Zhang, C.-L. He, G.-L. Shen and R.-Q. Yu, *Spectrochim. Acta, Part A*, 2008, 70, 337-342.

200 M. Shamsipur, M. Sadeghi, K. Alizadeh, H. Sharghi and R. Khalifeh, *Anal. Chim. Acta*, 2008, 630, 57-66.

201 C.-Y. Li, X.-B. Zhang, Z. Jin, R. Han, G.-L. Shen and R.-Q. Yu, *Anal. Chim. Acta*, 2006, 580, 143-148.

202 X. Wang, W. Zheng, H. Lin, G. Liu, Y. Chen and J. Fang, *Tetrahedron Lett.*, 2009, 50, 1536-1538.

203 X. Wang, W. Zheng, H. Lin and G. Liu, *J. Fluoresc.*, 2010, 20, 557-561.

204 F. G. Sánchez, A. Navas, J. J. Laserna and M. R. Martinez de la Barrera, *Z. Anal. Chem.*, 1983, 315, 491-495.

205 I. Mori, Y. Fujita, M. Toyoda, M. Hamada and M. Akagi, *Fresenius. J. Anal. Chem.*, 1992, 343, 902-904.

206 G. Zhang, S. Feng and D. Cheng, *Microchem. J.*, 1996, 53, 308-315.

207 I. Mori, K. Takasaki, Y. Fujita and T. Matsuo, *Talanta*, 1998, 47, 631-637.

208 Z. Zeng and R. A. Jewsbury, *Analyst*, 1998, 123, 2845-2850.

209 Q. Ma, Q.-E. Cao, Y. Zhao, S. Wu, Z. Hu and Q. Xu, *Food Chem.*, 2000, 71, 123-127.

210 S. H. Mashraqui, M. Chandiramani, R. Betkar and K. Poonia, *Tetrahedron Lett.*, 2010, 51, 1306-1308.

211 H. Y. Au-Yeung, E. J. New and C. J. Chang, *Chem. Commun.*, 2012, 48, 5268-5270.

212 W. Lin, L. Yuan, L. Long, C. Guo and J. Feng, *Adv. Funct. Mater.*, 2008, 18, 2366-2372.

213 N. Kaur and S. Kumar, *Tetrahedron Lett.*, 2008, 49, 5067-5069.

214 Y. Shiraishi, Y. Matsunaga and T. Hirai, *Chem. Commun.*, 2012, 48, 5485-5487.

215 E. J. Song, J. Kang, G. R. You, G. J. Park, Y. Kim, S.-J. Kim, C. Kim and R. G. Harrison, *Dalton Trans.*, 2013, 42, 15514-15520.

216 G. J. Park, Y. J. Na, H. Y. Jo, S. A. Lee and C. Kim, *Dalton Trans.*, 2014, 43, 6618-6622.

217 S. J. Zhen, F. L. Guo, L. Q. Chen, Y. F. Li, Q. Zhang and C. Z. Huang, *Chem. Commun.*, 2011, 47, 2562-2564.

218 Y. Yao, D. Tian and H. Li, *ACS Appl. Mater. Interfaces*, 2010, 2, 684-690.

219 K. D. Bhatt, D. J. Vyas, B. A. Makwana, S. M. Darjee and V. K. Jain, *Spectrochim. Acta, Part A*, 2014, 121, 94-100.

220 A. Sydor and D. Zamble, in *Metallomics and the Cell*, ed. L. Banci, Springer Netherlands, 2013.

221 S. W. Ragsdale, *J. Biol. Chem.*, 2009, 284, 18571-18575.

222 E. J. Calabrese, A. T. Canada and C. Sacco, *Annu. Rev. Public Health*, 1985, 6, 131-146.

223 A. Sharma, *Indian J. Dematol. Venereol. Leprol.*, 2007, 73, 307-312.

224 A. Sigel, H. Sigel and R. K. O. Sigel, *Nickel and Its Surprising Impact in Nature*, John Wiley & Sons Ltd.: U. K., 2007.

225 S. S. Brown and F. W. Sunderman, 1988, 1-4.

226 L. Fabbrizzi, M. Licchelli, P. Pallavicini, A. Perotti and D. Sacchi, *Angew. Chem. Int. Ed.*, 1994, 33, 1975-1977.

227 L. Fabbrizzi, M. Licchelli, P. Pallavicini, A. Perotti, A. Taglietti and D. Sacchi, *Chem. Eur. J.*, 1996, 2, 75-82.

228 F. Bolletta, I. Costa, L. Fabbrizzi, M. Licchelli, M. Montalti, P. Pallavicini, L. Prodi and N. Zaccheroni, *J. Chem. Sci. Dalton Trans.*, 1999, 1381-1386.
229 L.-J. Jiang, Q.-H. Luo, Z.-L. Wang, D.-J. Liu, Z. Zhang and H.-W. Hu, *Polyhedron*, 2001, 20, 2807-2812.
230 L. Salins, E. Goldsmith, M. Ensor and S. Daunert, *Anal Bioanal Chem*, 2002, 372, 174-180.
231 J. Zhao, B. A. Bertoglio, M. J. Devinney Jr, K. E. Dineley and A. R. Kay, *Anal. Biochem.*, 2009, 384, 34-41.
232 Q. Ke, T. Davidson, T. Kluz, A. Oller and M. Costa, *Toxicol. Appl. Pharmacol.*, 2007, 219, 18-23.
233 D. Cadosch, J. Meagher, O. P. Gautschi and L. Filgueira, *J. Neurosci. Meth.*, 2009, 178, 182-187.
234 H.-J. Thierse, S. Helm, M. Pink and H. U. Weltzien, *J. Immunol. Meth.*, 2007, 328, 14-20.
235 B. Wang, Y. Hu and Z. Su, *React. Funct. Polym.*, 2008, 68, 1137-1143.
236 B.-Y. Wang, X.-Y. Liu, Y.-L. Hu and Z.-X. Su, *Polym. Int.*, 2009, 58, 703-709.
237 S. C. Dodani, Q. He and C. J. Chang, *J. Am. Chem. Soc.*, 2009, 131, 18020-18021.
238 M. Y. Kang, C. S. Lim, H. S. Kim, E. W. Seo, H. M. Kim, O. Kwon and B. R. Cho, *Chem. Eur. J.*, 2012, 18, 1953-1960.
239 D. A. Pearce, G. K. Walkup and B. Imperiali, *Bioorg. Med. Chem. Lett.*, 1998, 8, 1963-1968.
240 N. Kaur and S. Kumar, *Chem. Commun.*, 2007, 3069-3070.
241 X. Liu, Q. Lin, T.-B. Wei and Y.-M. Zhang, *New J. Chem.*, 2014, 38, 1418-1423.
242 K. Hanaoka, *Chem. Pharm. Bull.*, 2010, 58, 1283-1294.

